COGNITIVE NEUROSCIENCE

Microglial Ffar4 deficiency promotes cognitive impairment in the context of metabolic syndrome

Wei Wang[1]†, Jinyou Li[2]†, Siyuan Cui[3], Jiayu Li[1], Xianlong Ye[4], Zhe Wang[1], Tingting Zhang[1], Xuan Jiang[1], Yulin Kong[1], Xin Chen[3], Yong Q. Chen[1]*, Shenglong Zhu[1,3]*

Metabolic syndrome (MetS) is closely associated with an increased risk of dementia and cognitive impairment, and a complex interaction of genetic and environmental dietary factors may be implicated. Free fatty acid receptor 4 (Ffar4) may bridge the genetic and dietary aspects of MetS development. However, the role of Ffar4 in MetS-related cognitive dysfunction is unclear. In this study, we found that *Ffar4* expression is down-regulated in MetS mice and MetS patients with cognitive impairment. Conventional and microglial conditional knockout of *Ffar4* exacerbated high-fat diet (HFD)–induced cognitive dysfunction and anxiety, whereas microglial *Ffar4* overexpression improved HFD-induced cognitive dysfunction and anxiety. Mechanistically, we found that microglial *Ffar4* regulated microglial activation through type I interferon signaling. Microglial depletion and NF-κB inhibition partially reversed cognitive dysfunction and anxiety in microglia-specific *Ffar4* knockout MetS mice. Together, these findings uncover a previously unappreciated role of Ffar4 in negatively regulating the NF-κB–IFN-β signaling and provide an attractive therapeutic target for delaying MetS-associated cognitive decline.

INTRODUCTION

Metabolic syndrome (MetS) has become a global health concern, accompanied by increasing prevalence in both absolute and relative numbers (*1*, *2*). It includes diabetes, fatty liver, obesity, and other metabolic disorders that produce a chronic inflammatory state and disordered lipid metabolism leading to hypertriglyceridemia, which extensively deteriorates the organs and tissues, including the central nervous system (CNS) (*3*–*5*). Epidemiological and clinical studies strongly suggest that MetS significantly increases the risk of dementia and cognitive decline (*6*–*8*). Genetic and environmental factors contribute to the development of MetS-related cognitive dysfunction, which is closely related to changes in lifestyle and dietary intake (*9*, *10*). Therefore, lifestyle changes and dietary modifications may represent an effective treatment approach. However, long-term controlled studies in humans are challenging, and the exact pathophysiological mechanism of MetS-related cognitive dysfunction remains ambiguous. Thus, given the importance of nutritional sensing in metabolic regulation, investigating the biological links between cognitive disorders and MetS through the lens of nutritional sensing is a potentially valuable avenue of research.

G protein–coupled receptors are the most druggable targets and have been studied extensively (*11*, *12*). In terms of free fatty acid receptors (FFARs), their activation plays an important role in diverse biological processes and has been implicated in regulating glucose or lipid metabolism (*13*, *14*). The currently identified members of the FFAR family include Ffar1 (GPR40), Ffar2 (GPR43), Ffar3 (GPR41), and Ffar4 (GPR120) (*15*), which may potentially bridge the gap between genetic and environmental factors in MetS-related cognitive dysfunction. Ffar2 and Ffar3 are mainly recognized and activated by short-chain fatty acids, while Ffar1 and Ffar4 are activated by medium- and long-chain fatty acids (LCFAs) (*15*). Ffar4 is widely expressed in various tissues and primarily serves as the receptor for LCFAs. Several studies have suggested that Ffar4 derived from different tissues may have biological distinctions (*16*–*18*). A detailed description of the physiological functions of Ffar4 in different tissues is essential and provides possible mechanisms underlying the contradictory findings of ω3 polyunsaturated fatty acid (PUFA) trials. The brain is rich in Ffar4 ligands (ω3 PUFAs), and its levels are associated with risks for dementia and related outcomes (*19*, *20*). The great majority of Ffar4 research has focused on the peripheral system, with little attention given to the potential contributions of the CNS. Therefore, the role of Ffar4, if any, in MetS-related cognitive dysfunction remains to be determined.

In the current study, we found that *Ffar4* was down-regulated in MetS mice and MetS patients with cognitive disorders. Specific deletion of *Ffar4* in microglia exacerbated MetS-related cognitive disorders and anxiety, while specific overexpression of *Ffar4* in microglia improved MetS-related cognitive disorders and anxiety. Mechanistically, we found that microglial Ffar4 negatively regulates microglial activation through type I interferon (IFN) signaling.

RESULTS

Decreased *Ffar4* expression is associated with cognitive impairment

To investigate the role of Ffar4 in MetS-related cognitive dysfunction, we analyzed *Ffar4* expression in two MetS models [high-fat diet (HFD) and db/db mice] and MetS patients with cognitive impairment. *Ffar4* expression in hippocampal tissue was significantly decreased in both mouse models, and the results of *Ffar4* expression in blood leukocytes were consistent with those in hippocampal tissue (Fig. 1, A and B). Analysis based on line regression also showed a negative correlation between hippocampal *Ffar4* expression and inflammatory cytokine expression (Fig. 1, C and D). To further establish the clinical relevance of *Ffar4*, we assessed *Ffar4* expression in human peripheral blood leukocytes derived from MetS patients without cognitive impairment, MetS patients with cognitive impairment, and healthy

[1]Wuxi School of Medicine, Jiangnan University, Wuxi 214000, China. [2]Affiliated Hospital of Jiangnan University, Wuxi 214122, China. [3]Jiangnan University Medical Center, Wuxi 214002, China. [4]Ganjiang Chinese Medicine Innovation Center, Nanchang 330000, China.
*Corresponding author. Email: shenglongzhu@jiangnan.edu.cn (S.Z.); yqchen@jiangnan.edu.cn (Y.Q.C.)
†These authors contributed equally to this work.

controls. We found a significant decreased *Ffar4* mRNA expression in peripheral blood leukocytes of MetS patients with cognitive impairment compared to MetS patients without cognitive impairment (Fig. 1E). In addition, a receiver operating characteristic (ROC) curve analysis was performed, and the results suggested that *Ffar4* might have diagnostic potential for MetS patients with cognitive impairment (Fig. 1F). Together, these results suggested that Ffar4 might have an important role in the pathophysiology of MetS-related cognitive impairments.

Ffar4 knockout exacerbates HFD-induced cognitive impairment and anxiety

To provide further insights into the role of Ffar4 in HFD induced neurobehavioral dysfunction, we generated a mouse model invalidated for the *Ffar4* gene (Fig. 2A and fig. S1A). The global MetS epidemic is generally believed to be caused by excessive caloric intake (*21*); thus, we used diet manipulations to induce MetS, such as male mice exposed to either a standard chow diet or 16 weeks of HFD (Fig. 2B). As expected, compared with standard chow-fed mice, mice fed an HFD for 16 weeks showed significant body weight gain and increased fasting blood glucose. HFD-fed mice exhibited higher plasma triglyceride (TG) and low-density lipoprotein (LDL) levels than standard chow-fed mice. However, we found that in the HFD state there was no significant difference between *Ffar4* knockout (KO) and wild-type (WT) mice (fig. S1, B to F). Next, we characterized the cognitive impairment and anxiety of these mice. As shown in Fig. 2 (C to G), HFD consumption significantly reduced center distance and entries into the center area in the open-field test (OFT). HFD/WT mice perform worse than their WT littermates in both the elevated plus maze (EPM) and light-dark box (LDB) tests, suggesting that HFD mice exhibited an anxiety phenotype compared with WT mice. HFD/*Ffar4*$^{-/-}$ mice showed a heightened anxiety behavioral phenotype compared to HFD/WT mice (Fig. 2, C to G). In the Morris water maze (MWM), HFD/WT mice spent more time reaching the platform in the training period, while KO of *Ffar4* significantly exacerbated task learning (Fig. 2H). Consistently, during the probe trial, HFD/*Ffar4*$^{-/-}$ mice crossed the platform fewer times than their littermate controls (Fig. 2, I and J). Together, these data suggested that *Ffar4* KO exacerbated HFD-induced anxiety and cognitive impairment.

Microglia-derived *Ffar4* mediates HFD-induced cognitive impairment and anxiety

Investigating which cell type–derived Ffar4 is involved in HFD-induced neurobehavioral dysfunction is the key to further exploring the mechanism. Given that Ffar4 is primarily present in microglia in

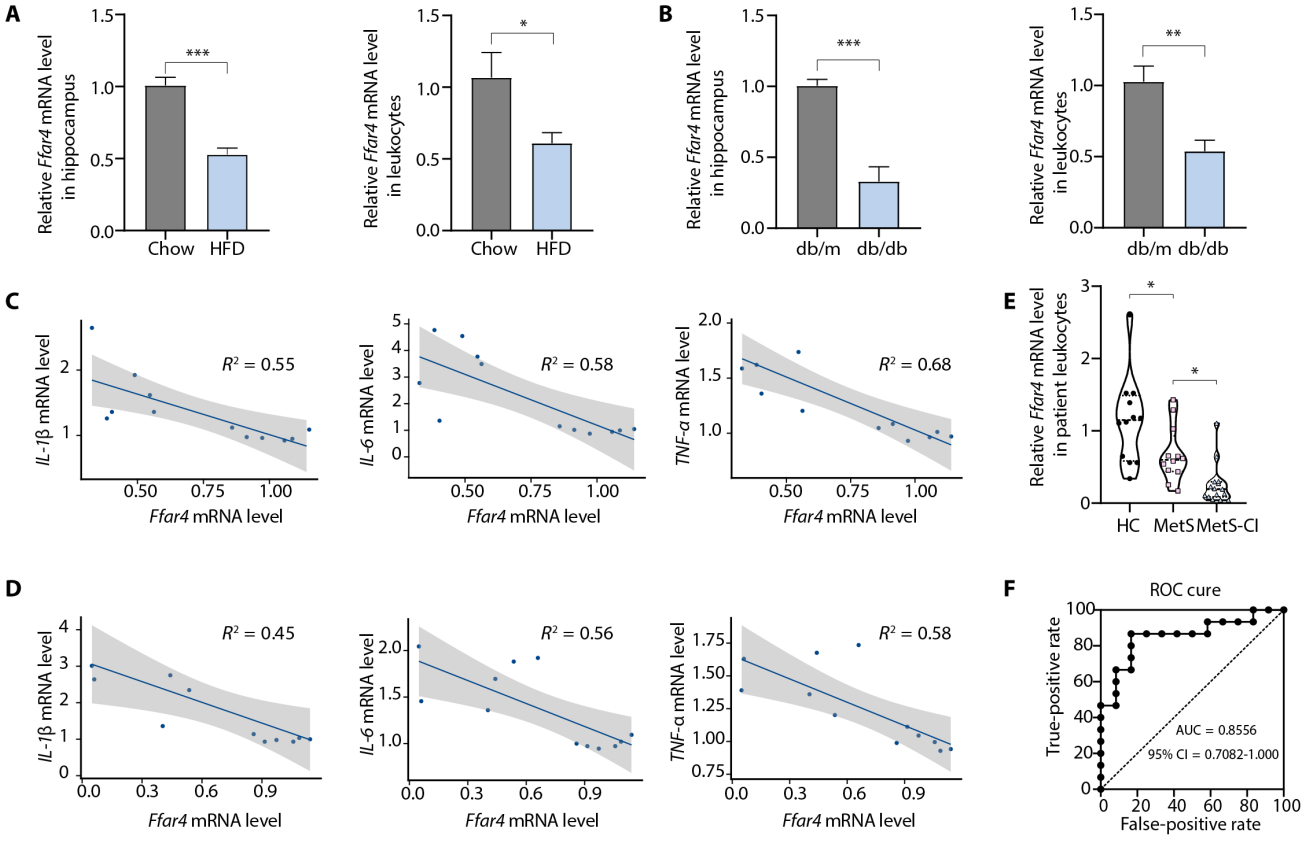

Fig. 1. *Ffar4* levels are decreased in MetS mice and MetS patients with cognitive impairment. (**A** and **B**) Two MetS models (HFD-induced obesity and diabetic db/db mice) and MetS patients with cognitive impairment were used, and qPCR was used to validate the levels of *Ffar4* mRNA in the hippocampal tissue and peripheral blood leukocytes of two MetS models ($n = 6$). Line regression was used to assess the correlation between hippocampal *Ffar4* expression and inflammatory cytokine expression in obese (**C**) and db/db mice (**D**). (**E**) Levels of *Ffar4* mRNA in human peripheral blood leukocytes derived from MetS patients with cognitive impairment ($n = 15$), without cognitive impairment ($n = 12$), and healthy controls ($n = 12$). (**F**) A ROC curve was used to assess the diagnostic value of *Ffar4* for MetS patients with cognitive impairment. Data are presented as means ± SEM. *$P < 0.05$. Detailed statistical analyses are presented in Materials and Methods. CI, confidence interval.

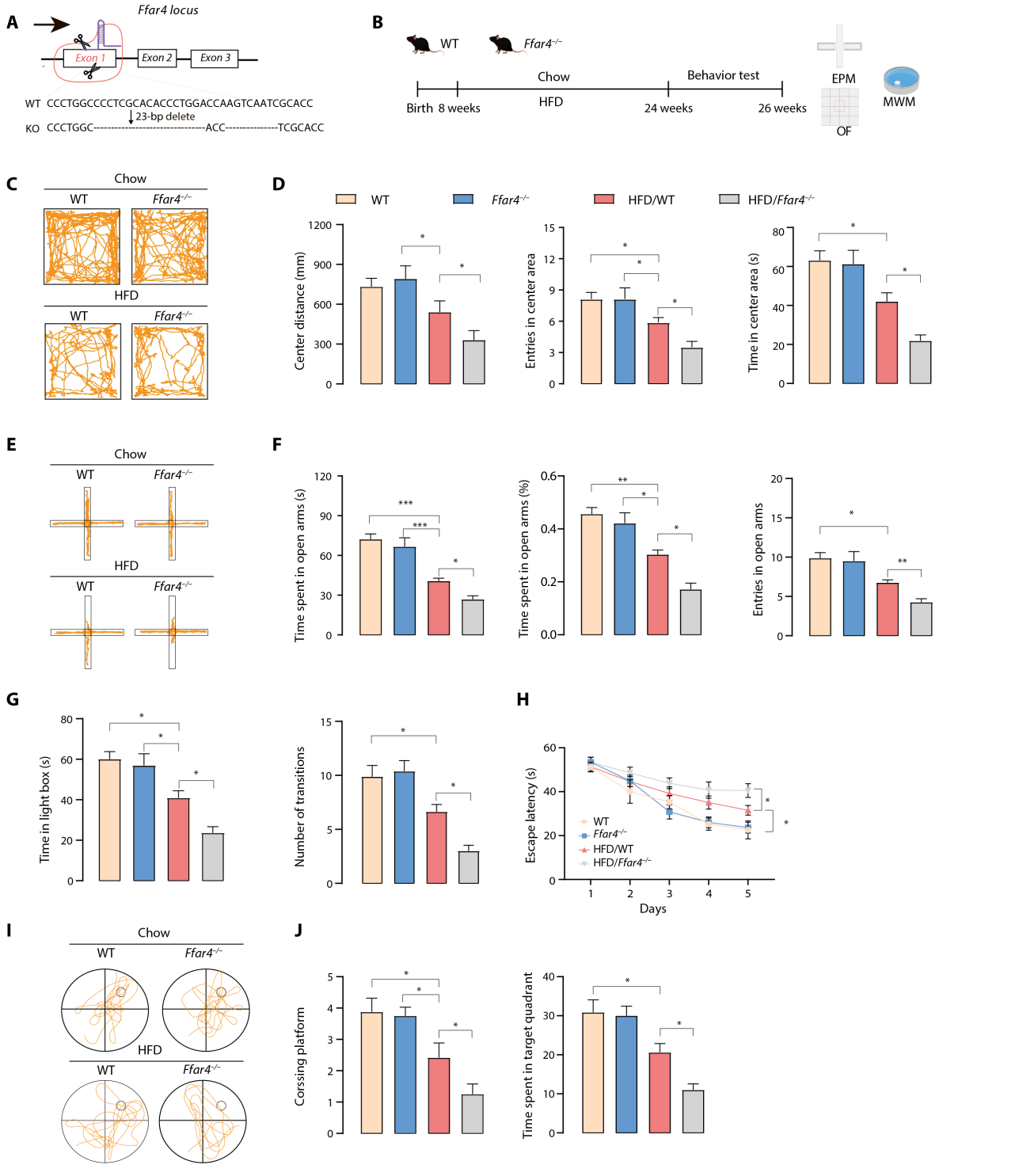

Fig. 2. *Ffar4* KO exacerbates HFD-induced neurobehavioral dysfunction. (**A**) CRISPR-Cas9 gene editing strategy for total *Ffar4* KO mice. (**B**) Schematic for HFD or chow feeding and behavioral testing. (**C**) Representative trajectory of mice in OFT. (**D**) Center distance, entries into the center area, and time in center area in the open field for WT, *Ffar4*$^{-/-}$, HFD/WT, and HFD/*Ffar4*$^{-/-}$ mice ($n = 7$ to 8 per group). (**E**) Representative trajectory of mice in EPM. (**F**) Time spent in the open zones of the mazes, time spent in open arms (%), and entries into the open area. (**G**) Time in light box and number of transitions in LDB. MWM analysis shows escape latency (**H**) to target in the invisible platform trials. Representative trajectory of mice in the probe trials (**I**), target cross number, and time spent in target quadrant (**J**) in the MWM test. Data are presented as means ± SEM. *$P < 0.05$, **$P < 0.01$, and ***$P < 0.001$. Detailed statistical analyses are presented in Materials and Methods.

the CNS (Fig. 3, A and B, and fig. S2A) (*22*, *23*), growing attention has been given to the effects and regulatory mechanisms of microglia. Thus, mice with tamoxifen-inducible microglial *Ffar4* conditional KO (cKO) were generated by crossing *Ffar4 flox/flox* mice with *Cx3cr1-CreER* transgenic mice, followed by tamoxifen injection (Fig. 3C). Their *Cx3cr1-CreER* littermates were used as controls. The HFD was started 4 weeks after the last tamoxifen injection to allow the replacement of peripheral monocytes (Fig. 3D). We isolated microglia from the brain and confirmed a high *Ffar4* KO efficiency (fig. S2, B and C). After 16 weeks HFD feeding, the levels of body weight, fasting blood glucose, plasma TG, and LDL were not significantly different between microglia-specific *Ffar4* KO mice and littermate control mice, except total cholesterol (TC) (fig. S2, D to H). To investigate the influence of microglial *Ffar4* cKO mice on MetS-related cognitive and anxiety functions, OFT, EPM, and MWM tests were conducted. As shown in Fig. 3 (E and F), cKO/HFD mice exhibited worse center distance and entries into center zone relative to littermate control mice. Similar results were observed in EPM; compared with the control/HFD mice, the time spent in the open arms and entries into open zones were significantly decreased in cKO mice (Fig. 3, G and H). cKO/HFD mice exhibited worse cognitive performance than control/HFD mice, as the cKO/HFD mice exhibited a longer escape latency and lower crossing frequency over the platform (Fig. 3, I to K). Together, these results demonstrated that microglial *Ffar4* was mainly responsible for exacerbating HFD-induced anxiety and cognitive impairment.

Microglia-specific *Ffar4* overexpression represses HFD-induced cognitive impairment and anxiety

To further corroborate the role of microglial *Ffar4* in HFD-induced neurobehavioral dysfunction, we crossed an *Ffar4 cag/cag* mouse strain with *Cx3cr1-CreER* transgenic mice to obtain microglial *Ffar4* conditional overexpression (cOE) mice (Fig. 4, A and B). After treatment of mice with tamoxifen for 4 weeks, we performed quantitative polymerase chain reaction (qPCR) to examine the expression level of *Ffar4* in the isolated microglia and confirmed a high *Ffar4* overexpression efficiency (fig. S3, A and B). After 16 weeks of HFD feeding, cOE mice displayed effectively reduced body weight, fasting blood glucose, plasma TG, and LDL compared with littermate control mice (fig. S3, C to G). We next performed behavioral experiments to assess the influence of microglia-specific *Ffar4* overexpression on MetS-related cognitive and anxiety functions. As shown in Fig. 4 (C and D), compared with the control/HFD group, the center distance in the open field and entries in the center zone were significantly increased in cOE/HFD mice. In addition, EPM results showed that cOE/HFD mice exhibited a significant increase in time spent in the open arms and entries into the open arms compared to control/HFD mice (Fig. 4, E and F). In the MWM test, we also found that cOE mice significantly decreased the latency to reach the platform and increased the number of platforms crossing (Fig. 4, G to I). These findings suggested that microglial *Ffar4* cOE alleviated HFD-induced anxiety and cognitive impairment and further demonstrated the role of microglial *Ffar4*.

Type I IFN signaling is enhanced in the absence of *Ffar4*

To further explore the potential molecular mechanism underlying the functions of Ffar4 in HFD-induced anxiety and cognitive impairment, we isolated primary microglia from cKO/HFD mice and compared them from control/HFD mice (Fig. 5A). A total of 225 up-regulated genes and 345 down-regulated genes were identified in the microglia of cKO/HFD mice (Fig. 5, B and C), and the Gene Ontology (GO) analysis that was underrepresented in the cKO/HFD mice was related to the negative regulation of type I IFN production (Fig. 5, D and E). Type I IFNs (mainly IFN-α and IFN-β) bind to the cell surface complex known as IFN-α/β receptor and then activate Janus kinase 1 (JAK1)/signal transducer and activator of transcription 1 (STAT1) signal transducer, leading to an inflammatory response. One characteristic of microglia in neurodegeneration is the increased production of inflammatory cytokines. We found that microglia from cKO/HFD mice showed only increased *IFN*-β mRNA expression compared with age-matched littermate control mice, while having no effect on *IFN*-α (Fig. 5F). Furthermore, using enzyme-linked immunosorbent assay (ELISA), we found that IFN-β was also significantly increased in cKO/HFD mice (Fig. 5G). The phosphorylation of JAK1 and STAT1 was significantly up-regulated in the hippocampus of cKO/HFD mice (Fig. 5H). We next examined whether blocking type I IFN signaling could improve cognitive impairment and anxiety behavior in cKO/HFD mice. The administration of fludarabine, a widely used type I IFN signaling inhibitor (*24*–*26*), improved cognitive impairment and decreased anxiety-like behavior comparably to cKO/HFD mice (fig. S4). Together, these results indicated that microglial *Ffar4* could regulate type I IFN signaling pathway in HFD-induced cognitive impairment and anxiety.

Microglial *Ffar4* deletion aggravates neuroinflammation caused by microglial activation

To investigate the role of microglial *Ffar4* KO in neuroinflammation, we analyzed inflammatory cytokines and microglial morphological changes. Control/HFD mice showed a significantly different morphology, characterized by decreased total branch length, average branch length, branch numbers, and terminal numbers. Notably, microglial *Ffar4* KO markedly aggravated HFD-induced morphological changes (Fig. 6, A and B). In addition, we quantified the levels of CD68, a lysosome marker indicating the phagocytosis activity of microglia, and found that the density of CD68 was significantly increased in the Ffar4 KO microglia, suggesting higher phagocytic capacity (Fig. 6C). Next, we analyzed the effect of *Ffar4* on inflammatory cytokines. As expected, microglial *Ffar4* KO markedly increased the levels of some proinflammatory cytokines (*Arg-1*, *IL-10*, and *TGF*-β) and increased the levels of interferon-stimulated gene (ISG)-related gene (*CXCL-10* and *Isg-15*) (Fig. 6, D and E). In contrast, microglial *Ffar4* overexpression could significantly inhibit inflammatory cytokines and ISG-related gene expression (fig. S5). We further investigated the effect of inflammatory response on synapses. Western blotting revealed that the expression of the presynaptic protein synaptophysin (SYN) and the postsynaptic protein PSD95 was significantly down-regulated in the hippocampus of cKO/HFD mice (Fig. 6F). Consistent with this finding, microglial *Ffar4* KO further exacerbated cell apoptosis (Fig. 6F). To corroborate our finding that microglial *Ffar4* regulates type I IFN signaling in vivo, we isolated primary microglia from WT mice and *Ffar4* KO mice and treated them with palmitic acid (Fig. 6G). In agreement with the animal results, *Ffar4* deletion significantly increased palmitic acid–induced *IFN*-β, *CXCL-10*, *Isg-15*, *IL-6*, and *IL-1*β production (Fig. 6H). We investigated whether *IFN*-β silencing blocked the proinflammatory effects. As expected, *IFN*-β silencing significantly suppressed the *Ffar4* deficiency–induced increase in *IFN*-β, *CXCL-10*, *Isg-15*, *IL-6*, and *IL-1*β (Fig. 6I). To elucidate the role of microglia in behavioral

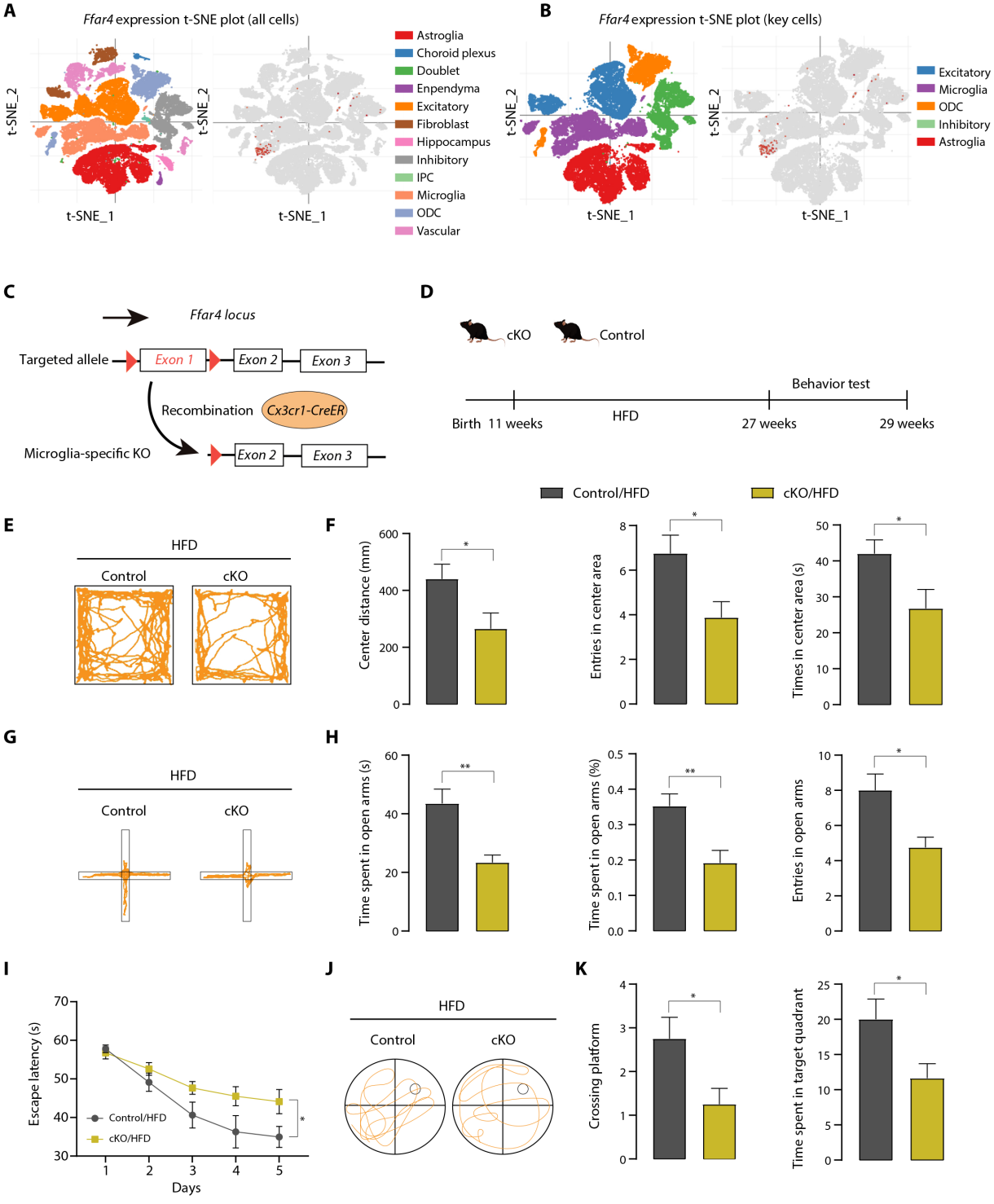

Fig. 3. Microglial *Ffar4* KO exacerbates HFD-induced neurobehavioral dysfunction. (**A** and **B**) T-distributed stochastic neighbor embedding (t-SNE) plot of mouse cortex cells (visualization available at https://singlecell.broadinstitute.org/). (**C**) Gene targeting strategy for microglia-specific *Ffar4* KO. Mice with floxed exon 1 of *Ffar4* were generated by homologous recombination. Microglial-specific *Ffar4* knockout (cKO) mice were obtained by mating with *Cx3cr1-CreER* mice. (**D**) Schematic for HFD or chow feeding and behavioral testing. (**E**) Representative trajectory of mice in OFT. (**F**) Center distance, entries into the center area, and time in center area in the open field for control/HFD and cKO/HFD mice ($n = 8$ per group). (**G**) Representative trajectory of mice in EPM. (**H**) Time spent in the open zones of the mazes, time spent in open arms (%), and entries into the open area. MWM analysis shows escape latency (**I**) to target in the invisible platform trials. Representative trajectory of mice in the probe trials (**J**) and target cross number, and time spent in target quadrant (**K**) in the MWM test. Data are presented as means ± SEM. $^{*}P < 0.05$, $^{**}P < 0.01$, and $^{***}P < 0.001$. Detailed statistical analyses are presented in Materials and Methods.

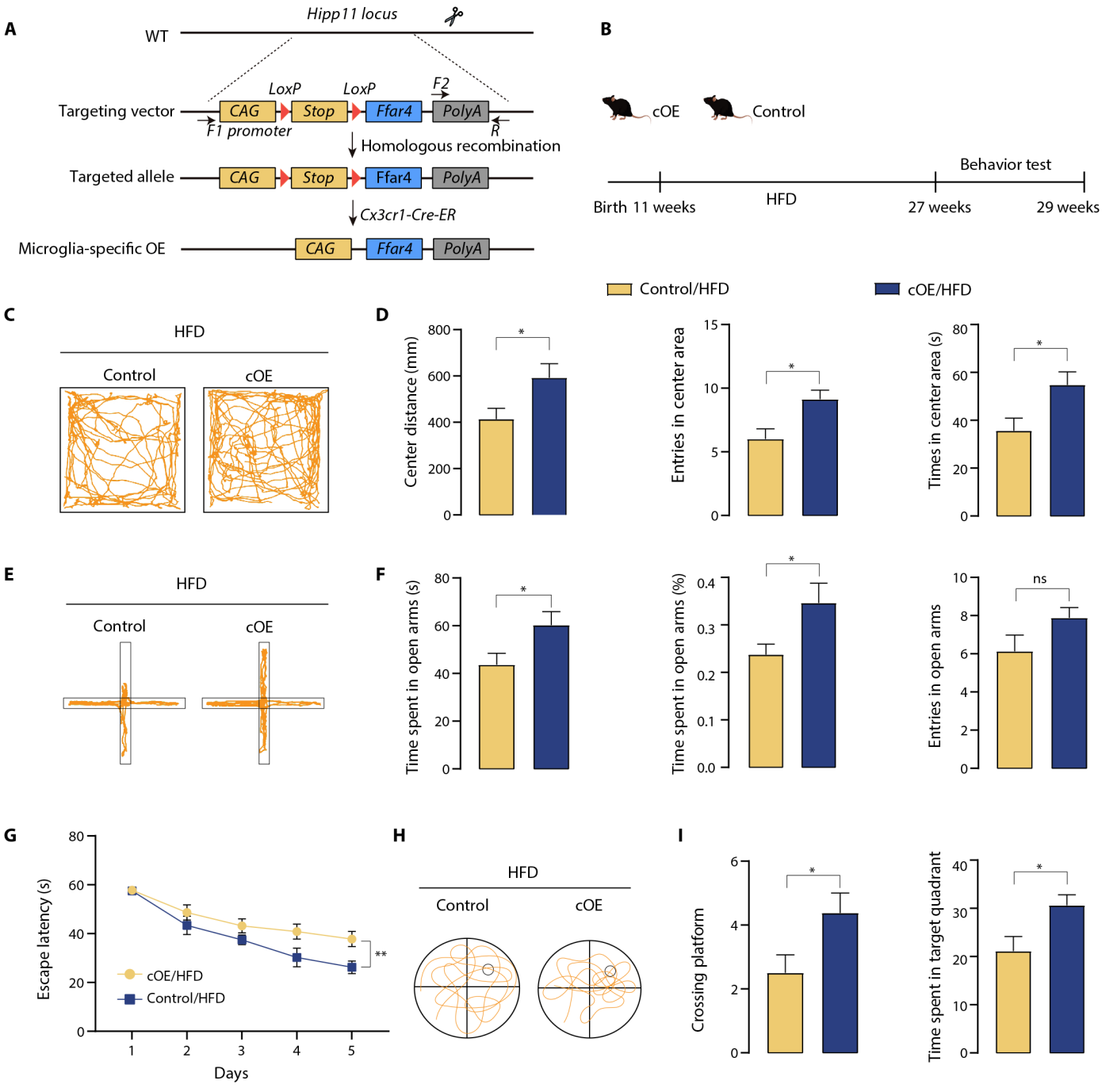

Fig. 4. Microglial *Ffar4* overexpression restores HFD-induced neurobehavioral dysfunction. (**A**) Transgenic strategy for microglial-specific *Ffar4* expression. The floxed *Ffar4* expression cassette was targeted to the *Hipp11* locus by homologous recombination. Microglial-specific *Ffar4*-expressing mice (cOE) were obtained by mating with *Cx3cr1-CreER* mice, which removes the *STOP* fragment. (**B**) Schematic for HFD or chow feeding, and behavioral testing. (**C**) Representative trajectory of mice in OFT. (**D**) Center distance, entries into the center area, and time in center area in the open field for control/HFD and cOE/HFD mice ($n = 8$ per group). (**E**) Representative trajectory of mice in EPM. (**F**) The time spent in the open zones of the mazes, time spent in open arms (%), and entries into the open area were measured to evaluate anxiety. MWM analysis shows escape latency (**G**) to target in the invisible platform trials. Representative trajectory of mice in the probe trials (**H**) and target cross number, and time spent in target quadrant (**I**) in the MWM test. Data are presented as means ± SEM. *$P < 0.05$. Detailed statistical analyses are presented in Materials and Methods. ns, not significant.

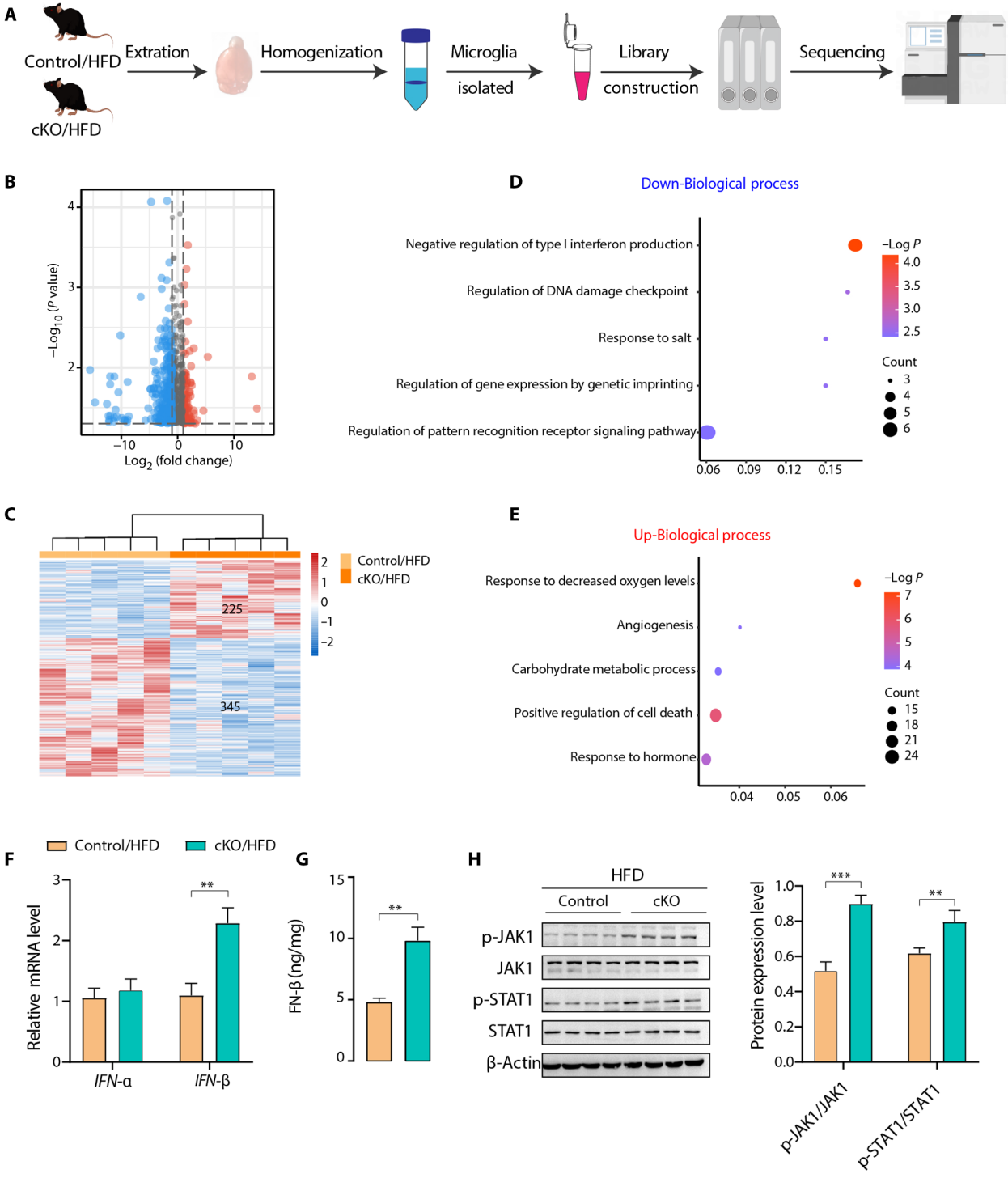

Fig. 5. Microglial transcriptome analysis suggests that *Ffar4* regulate type I IFN signaling. (**A**) Schematic for microglia isolation, RNA extraction, RNA-seq, and data analysis. Volcano plot (**B**) and heatmap (**C**) show the distribution of up-regulated (red) and down-regulated (blue) genes. GO enrichment analysis of (**D**) down-regulated (blue) and (**E**) up-regulated (red) genes. (**F**) qPCR assay to test the expression levels of type I IFNs (*IFN*-α and *IFN*-β) in isolated microglial cells from control/HFD and cKO/HFD mice ($n = 6$ per group). (**G**) ELISA analysis of *IFN*-β contents in hippocampal tissue from these two groups of mice ($n = 6$ per group). (**H**) Immunoblotting and statistical analysis of JAK1, p-JAK1, STAT1, and p-STAT1 levels in hippocampal tissue from these two groups of mice ($n = 4$ per group). Data are presented as means ± SEM. $^{**}P < 0.01$ and $^{***}P < 0.001$. Detailed statistical analyses are presented in Materials and Methods. Illustration in (A) created with Figdraw.

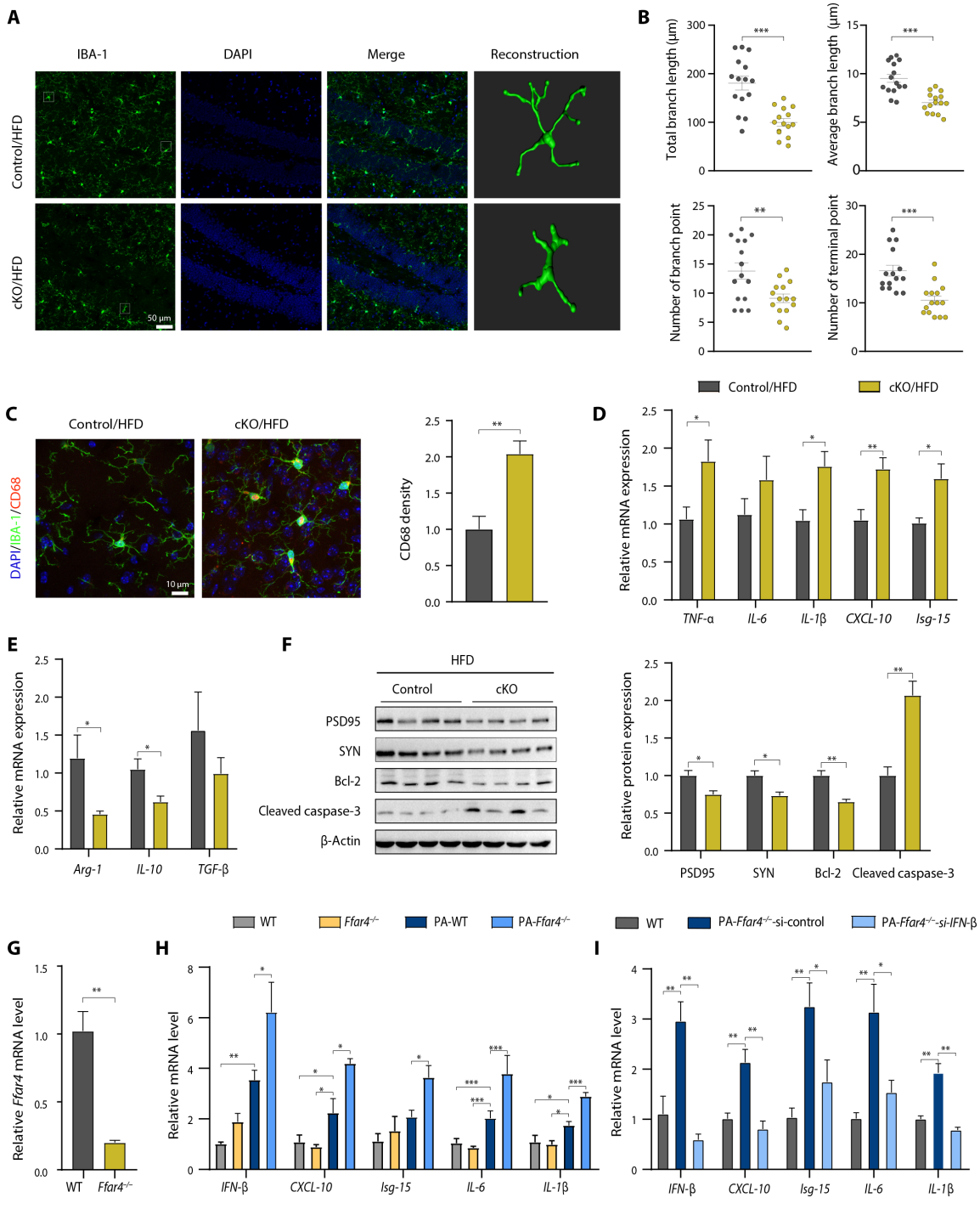

Fig. 6. Microglial *Ffar4* KO increases microglial activation. (**A**) Representative images of Iba-1–positive cells in the hippocampal DG of control/HFD and cKO/HFD groups with three-dimensional (3D) reconstruction of representative microglia using Imaris. Scale bar, 50 μm. (**B**) Microglial morphology as total branch length, average branch length, branch numbers, and terminal numbers in the control/HFD and cKO/HFD groups ($n = 15$ from three mice per group). (**C**) Immunofluorescent staining of Iba-1 and CD68 and statistical analysis of CD68 level in the control/HFD and cKO/HFD groups. Scale bar, 10 μm. $n = 6$ per group. (**D** and **E**) qPCR assay to test the expression levels of pro- and anti-inflammatory cytokines and ISG-related gene in isolated microglial cells from control/HFD and cKO/HFD mice ($n = 6$ per group). (**F**) Immunoblotting and statistical analysis of SYN, PSD95, cleaved caspase-3, and Bcl-2 in hippocampal tissue from the control/HFD and cKO/HFD groups ($n = 4$ per group). (**G**) *Ffar4* mRNA level in microglia isolated from WT and *Ffar4* KO mice ($n = 3$ per group). (**H**) qPCR assay to test the expression levels of *IL-1β*, *IL-6*, *CXCL-10*, *IFN-β*, and *Isg-15* under palmitic acid (200 μM) incubation for 24 hours in primary microglial cell cultures of WT and *Ffar4* KO mice ($n = 3$). (**I**) After *IFN-β* siRNA was transfected into microglia, qPCR was used to test the expression levels of *IL-1β*, *IL-6*, *CXCL-10*, *IFN-β*, and *Isg-15* under palmitic acid (200 μM) incubation for 24 hours in primary microglial cell cultures of WT and *Ffar4* KO mice ($n = 3$). Data are presented as means ± SEM. $^*P < 0.05$, $^{**}P < 0.01$, and $^{***}P < 0.001$. Detailed statistical analyses are presented in Materials and Methods.

abnormalities of cKO/HFD mice, we took advantage of pharmacological microglia deletion using PLX3397, a colony-stimulating factor 1 receptor (CSF1R) inhibitor, to assess the consequence of microglia elimination on cognitive function and anxiety behavior (*27*–*29*). Results showed that PLX3397 treatment markedly reduced the number of Iba-1–positive microglia in the hippocampus (fig. S6). In addition, PLX3397 treatment rescued the cognitive impairment and anxiety-related behaviors of cKO/HFD mice (fig. S6). Together, these results demonstrated that microglial Ffar4 played a key role in HFD and palmitic acid–induced inflammatory responses.

Ffar4 regulates *IFN*-β transcription via NF-κB

IFN-β production relies on three transcription factor complexes: Interferon regulatory factor 3 (IRF-3) binds positive regulatory domains I and II (PRDI and PRDIII), the NF-κB complex binds PRDII, and the ATF-2/c-Jun AP-1 complex binds PRDIV (*30*). Thus, we first evaluated the mRNA levels of *IRF-3*, *NF-κB*, and *ATF2* in microglia from cKO/HFD and control/HFD mice, and the results indicated that only the mRNA levels of *NF-κB* in the cKO/HFD mice were markedly increased compared with those in the control/HFD mice (fig. S7A). We next determined whether the NF-κB pathway activated microglial *IFN*-β transcription in primary microglia by using PDTC, a specific NF-κB inhibitor with blood-brain barrier permeability. *Ffar4*-KO microglia were treated with palmitic acid with or without PDTC cotreatments, and significant reductions in *IFN*-β, *CXCL-10*, *Isg-15*, *IL-6*, and *IL-1*β production were observed in *Ffar4*-KO microglia treated with PDTC (fig. S7B). In *Ffar4* KO microglial cells cultured with PDTC and palmitic acid, the phosphorylation of NF-κB, JAK1, and STAT1 was significantly down-regulated (fig. S7, C and D). Given the in vitro findings of NF-κB in *IFN*-β transcription and JAK1/STAT1 signaling, we next determined the effect of the pharmacological blockade of NF-κB on cKO/HFD mice (Fig. 7A). PDTC intervention significantly ameliorated HFD-induced anxiety and cognitive dysfunction in cKO mice (Fig. 7, B to G). cKO-induced increases in *TNF*-α, *IL-1*β, and *IFN*-β levels and reductions in *Arg-1* and *TGF*-β levels were abolished by treatment with PDTC (Fig. 7, H to K). We next checked whether PDTC intervention influenced the activity of microglia in HFD-cKO mice. As shown in Fig. 7 (L and M), significant increases in total branch length, average branch length, branch numbers, and terminal numbers were observed in PDTC-treated mice. We found that PDTC intervention inhibited the phosphorylation of NF-κB, JAK1, and STAT1 in the hippocampus of cKO mice (Fig. 7N). Furthermore, PDTC intervention attenuated HFD-induced synaptic damage and cell apoptosis in cKO mice (Fig. 7O). As previously described, Ffar4 could recruit β-arrestin-2, leading to internalization of the receptor, and inhibits activation of NF-κB (*31*–*33*). This study also confirmed the direct interactions between Ffar4 and β-arrestin-2 in microglial via immunoprecipitation (IP) assay (Fig. 7P). In addition, either *Ffar4* or β-*arrestin-2* knockdowns resulted in the NF-κB activation, suggesting the vital role of Ffar4 signaling in NF-κB modulation (Fig. 7Q and fig. S7C). Furthermore, protein-DNA interaction was analyzed using CUT&RUN (cleavage under targets and release using nuclease) assay to examine direct mechanism by which Ffar4 regulates the interactions between NF-κB and *IFN*-β, and the results showed increased binding of NF-κB to the *IFN*-β promoter after knockdown of *Ffar4* (Fig. 7R). Meanwhile, given the strong response to Ffar4 in regulating microglial activation, we next evaluated the therapeutic potential of pharmacologically targeting Ffar4 and NF-κB in BV2 cells and primary microglia. Ffar4 agonists have been developed and appear to be well tolerated in mice. However, the clinical safety of these drugs remains to be demonstrated. Dietary intake of polyunsaturated fatty acids may be a potential mechanism. To test this hypothesis, we incubated BV2 cells and primary microglia with DHA or PDTC. Microglia preincubated with DHA and PDTC exhibited weakened palmitic acid–induced NF-κB activation, *IFN*-β, and inflammatory cytokine production (fig. S8, A and B). Notably, DHA therapy was significantly superior to PDTC alone in *IFN*-β–producing primary microglia and BV2 cells (fig. S8, A and B). This suggests that DHA may regulate IFN production in a variety of ways, not just through NF-κB. Moreover, while PDTC inhibited NF-κB activation, it had a less powerful effect on p-STAT1 and p-JAK1 levels than DHA, which indicated that PDTC could only regulate type through the NF-κB approach (fig. S8, C and D). Together, our data suggest that Ffar4 might represent an effective therapy for microglial inflammatory response.

DISCUSSION

Clinically, a critical comorbidity of cognitive impairment in patients with metabolic disorders is diminished or lost attention, memory, perceptual, and executive ability, leading to functional impairment and reduced quality of life (*34*, *35*). Although various pathological theories have been proposed, the underlying mechanisms of MetS-induced neurobehavioral changes are not fully understood, resulting in a lack of successful treatment methods. In the present study, we identified a potential role of *Ffar4* in MetS-induced cognitive impairment and anxiety and explored the mechanism of this role in vitro and in vivo. Our results provide evidence that decreased *Ffar4* expression is associated with cognitive impairment and that microglial *Ffar4* deficiency significantly exacerbates HFD-induced neuro behavioral disorders, while conditional microglial *Ffar4* overexpression improves HFD-induced neurobehavioral disorders, and microglial Ffar4 regulates type I IFN signaling through NF-κB. Blockade of NF-κB combined with Ffar4 activation provides a strategy for neuroinflammation therapy (Fig. 8).

Several epidemiological studies and randomized controlled trials have elucidated the effect of omega-3 PUFA interventions on cognitive function, but the published results of these studies are inconsistent (*36*–*38*). Studies have failed to demonstrate a beneficial effect of omega-3 PUFA supplementation in patients with moderate or severe Alzheimer's disease (AD) (*39*), but in patients with mild AD or mild cognitive impairment (MCI) (*40*). Another possible explanation for this difference is the variation in genetic variants of *Ffar4*. As the receptor of omega-3 PUFAs, the *p.R270H* variant of the *Ffar4* gene is associated with loss of function, reduced protein activity, and increased risk of metabolic disorders (*41*, *42*). Therefore, genetic variants of *Ffar4* may be a reason for the inconsistent results of clinical trials, suggesting that future clinical trials should consider including *Ffar4* genetic variations in the population. In this study, we found that *Ffar4* mRNA levels were down-regulated in MetS mice and MetS patients with cognitive impairment. Many LCFAs can bind to Ffar4, which may produce different effects, as Ffar4 can recognize the double bond in fatty acids and cause different downstream signaling pathways (*43*). Therefore, the exact role of Ffar4 in the CNS is still unclear. Here, using genetic methods, we observed that microglial *Ffar4* ablation exacerbated HFD-induced cognitive impairment and anxiety.

Ffar4 has been found to regulate the secretion of glucagon-like peptide-1 (GLP-1) in intestinal endocrine cells (*41*, *44*). GLP-1

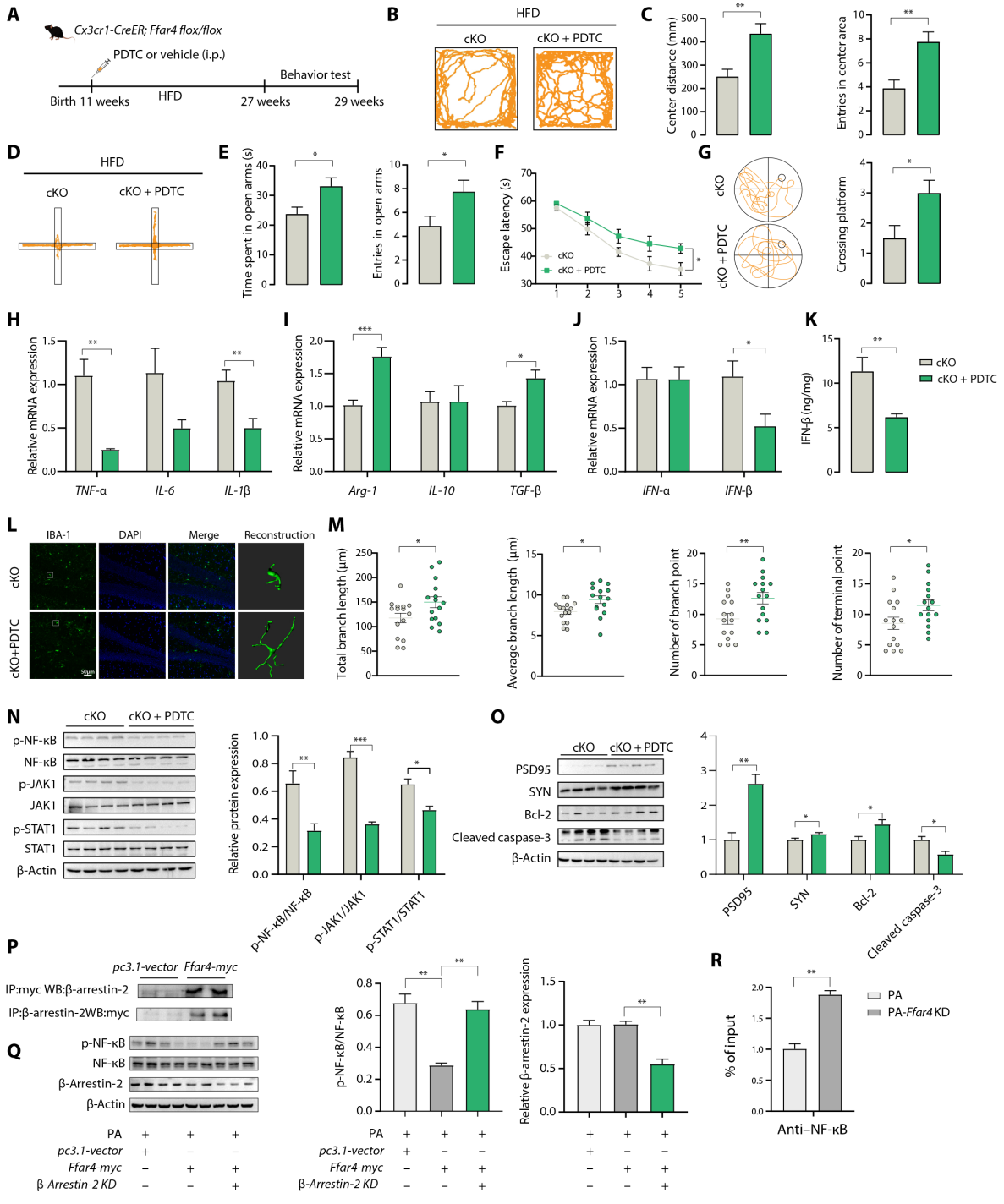

Fig. 7. NF-κB inhibitor PDTC restores neurobehavioral dysfunction. (**A**) Experimental flow chart. i.p., intraperitoneal. (**B**) Representative trajectory of mice in OFT. (**C**) Center distance and entries into the center area traveled in the open field ($n = 8$). (**D**) Representative trajectory of mice in EPM. (**E**) Time spent in the open zones of the mazes and entries into EPM. MWM analysis shows escape latency (**F**) to target in the invisible platform trials. (**G**) Representative trajectory of mice in the probe trials and target cross number in the MWM test. (**H** and **I**) mRNA expression levels of pro- and anti-inflammatory cytokines in isolated microglial cells from cKO and cKO/PDTC mice ($n = 6$). (**J**) Expression levels of type I IFNs ($n = 6$). (**K**) ELISA analysis of *IFN*-β content in hippocampal tissue ($n = 6$). (**L**) Representative images of Iba-1–positive cells in the hippocampal DG with 3D reconstruction using Imaris. Scale bar, 50 μm. (**M**) Microglial morphology as total branch length, average branch length, branch numbers, and terminal numbers ($n = 15$ from three mice per group). (**N**) Immunoblotting and statistical analysis of p–NF-κB/NF-κB, p-JAK1/JAK1, and p-STAT1/STAT1 levels in hippocampal tissue ($n = 4$). (**O**) Immunoblotting and statistical analysis of SYN, PSD95, cleaved caspase-3, and Bcl-2 in hippocampal tissue ($n = 4$). (**P**) Interaction between Ffar4-myc and β-arrestin-2 in BV2 cells. (**Q**) The knockdown of β-*arrestin-2* increased the NF-κB activation. Immunoblotting and statistical analysis of NF-κB, p–NF-κB, and β-arrestin-2 level in BV2 cells ($n = 3$). (**R**) CUT&RUN assay–validated NF-κB binds to target *IFN*-β promoter after *Ffar4* knockdown ($n = 3$). Data are presented as means ± SEM. $^*P < 0.05$, $^{**}P < 0.01$, and $^{***}P < 0.001$. Detailed statistical analyses are presented in Materials and Methods.

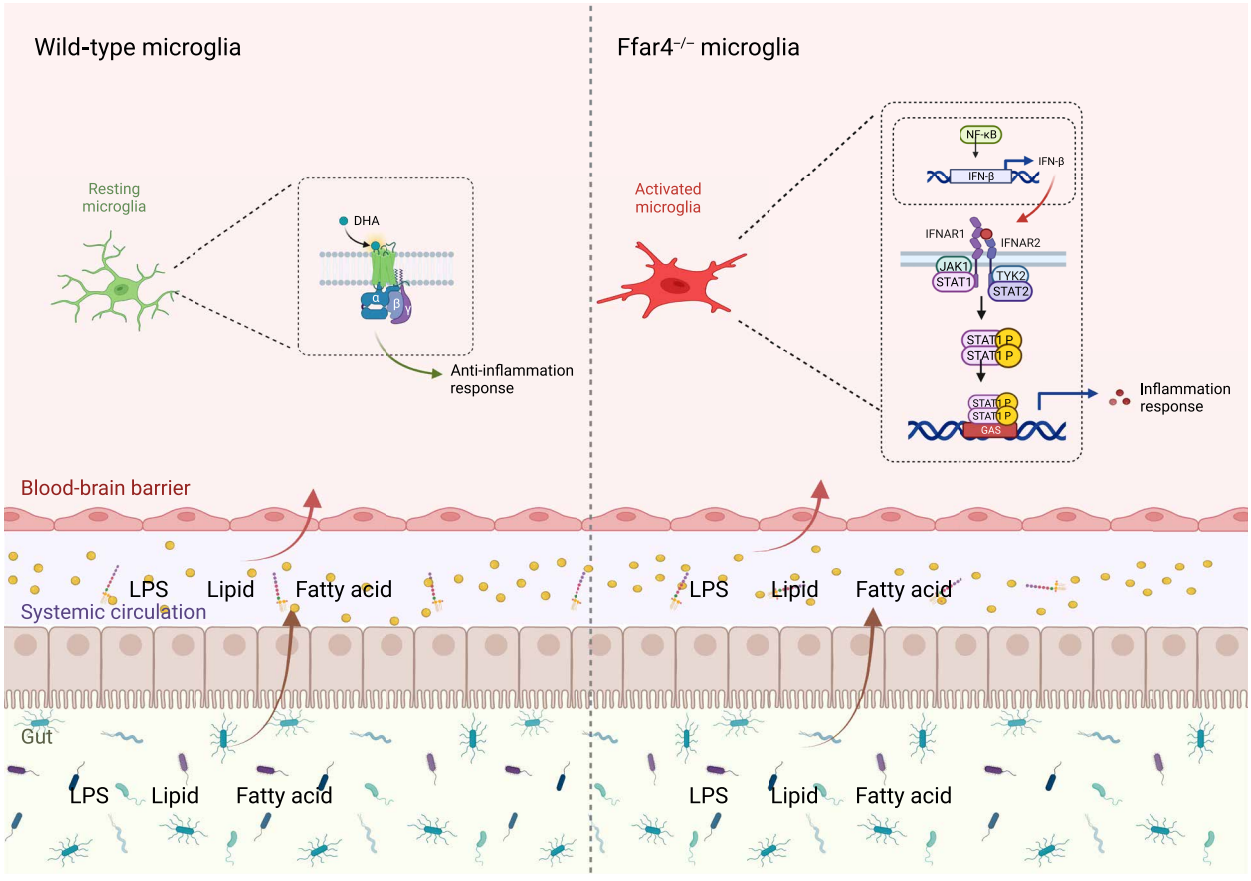

Fig. 8. Schematic of the mechanism by which microglial *Ffar4* deletion induces microglial reactivity. Illustration created with BioRender.com

exhibits excellent effects in combating MetS. In addition to regulating the peripheral system, GLP-1 can also cross the blood-brain barrier to increase neuronal activity, promote neuronal growth, and improve learning and memory (*45*, *46*). Furthermore, the latest clinical trials have found that MetS patients receiving GLP-1 agonists have a 53% reduced risk of developing dementia (*47*). This may indirectly result from the regulation of GLP-1 release in intestinal endocrine cells by Ffar4 in the gut (*44*, *48*). Our research findings further expand the direct role of Ffar4 in cognitive function. Here, we propose the following regulatory pathway: Microglial *Ffar4* deficiency activates NF-κB, leading to *IFN*-β transcriptional activation, followed by activation of JAK1/STAT1 signaling and subsequent exacerbation of HFD-induced neurobehavioral disorders.

NF-κB regulates metabolic processes at multiple levels in conjunction with NF-κB–mediated transcriptional events, making it a suitable potential therapeutic target for MetS (*49*). However, targeted toxicity due to systemic NF-κB blockade greatly limits the efficacy and clinical promotion of NF-κB (*50*). DHA, which is the main omega-3 PUFA in the brain, can normalize saturated fatty acid–induced harmful effects (*32*). Our results showed that combined treatment with NF-κB and Ffar4 was more effective than monotherapy. However, whether this combination approach has therapeutic potential in humans remains to be determined. Although DHA plays a major role in vitro, it is important to note that DHA lacks specificity, and the maximum biological activity of orally administered DHA in the population is still unclear, which may weaken the therapeutic efficacy of DHA in clinical trials. On the basis of this, targeted Ffar4 agonists show great potential for the treatment of MetS-related cognitive disorders.

In summary, our study suggests that microglial *Ffar4* deficiency contributes to the development of MetS-related cognitive disorders and anxiety, describes a mechanism by which microglial *Ffar4* regulates type I IFN signaling through NF-κB–*IFN*-β signaling, and may provide potential therapeutic strategies for managing anxiety and cognitive disorders induced by MetS. Furthermore, the development of Ffar4-specific agonists and tissue-specific delivery methods may be promising approach for treating neurological diseases.

MATERIALS AND METHODS

Human participants

Peripheral blood samples were obtained from 15 patients with type 2 diabetes with cognitive impairment, 12 patients with type 2 diabetes without cognitive impairment, and 12 patients with healthy controls. All type 2 diabetes participants fulfilled the diagnostic criteria for type 2 diabetes according to American Diabetes Association classification. The Montreal Cognitive Assessment (MoCA) was used to assess participant's cognitive function, and overall score < 26 indicated cognitive impairment. Human peripheral RNA samples were used to assess FFAR4 mRNA expression by reverse transcription qPCR (RT-qPCR). This study was approved by the Medical Ethics Committee

of Jiangnan University (reference no. JNU20210310IRB01). All participants signed informed consent before the study.

Animals and study design

All mice used were from the C57BL/6J genetic background. *Ffar4* total KO [Research Resource Identifier (RRID): MGI:7256540] mice were purchased by Shanghai Bioray Lab. The tail tips were digested with 150 μl of NaOH (50 mM) at 95°C for 15 min, followed by the neutralization with 10 μl of tris-HCl (pH 8.0). Using the forward primer CCCGGCATGTCCCCTGAGTGT and the reverse primer TGGTCGCCCTTGACATCCGAGA at 95°C for 30 s and 63°C for 45 s for 40 cycles, *Ffar4* KO mice were genotyped by PCR using tail DNA. WT mice generated an 87–base pair (bp) gene fragment, and *Ffar4* mice generated a 110-bp gene fragment. Floxed *Ffar4* (fl/fl; RRID: MGI: 7256541) mouse models were established by Shanghai Biomodel Organism. *Cx3cr1-CreER* mice on the C57BL/6J background were obtained from C. X. Tang (Xuzhou Medical University, China) and maintained at Jiangnan University. *Ffar4 (fl/fl)* mice were identified using the forward primer TGCTCTTTCTGGAGCTGTGT and the reverse primer AGAGATCAGAATGGACAACT by PCR using tail DNA at 95°C for 30 s, 58°C for 45 s, and 72°C for 30 s for 40 cycles. WT mice generated a 243-bp gene fragment, and *fl/fl* mice generated a 272-bp gene fragment. *Ffar4* overexpression transgenic mice were genotyped using forward primer 1: CAGCAAAACCTGGCTGTGGATC, forward primer 2: GTGGAGTCCCATCATCATCACC, and the reverse primer: ATGAGCCACCATGTGGGTGTC at 95°C for 30 s, 65°C (−0.5°C per cycle) for 30 s, and 72°C for 45 s for 20 cycles and then 95°C for 30 s, 55°C for 30 s, and 72°C for 45 s for 20 cycles, generating a 1051-bp fragment for cag/cag and a 243-bp fragment for the WT. Microglia cell–specific *Ffar4*-KO mice (cKO) were obtained by crossing *fl/fl* mice with *Cx3cr1-CreER* mice. Microglia cell–specific *Ffar4* overexpression mice were obtained by crossing *cag/cag* mice with *Cx3cr1-CreER* mice. To induce Cre-mediated recombination, all 6-week-old mice (*Ffar4 fl/fl*: *Cx3cr1-CreER*; *Ffar4 cag/cag*: *Cx3cr1-CreER*) and their littermate controls (*Ffar4* w/w: *Cx3cr1-CreER*) were treated with tamoxifen (20 mg/ml; MedChemExpress, HY-13757A) in corn oil (MedChemExpress, HY-Y1888) via intraperitoneal injection, once each day for 5 days at a dose of 100 μl per injection (*51*, *52*). Animals were provided a standard chow diet or HFD (60% fat; Research Diet, Rodent Chow D12451) and water ad libitum unless otherwise stated. HFD was started 4 weeks from the last tamoxifen injection to allow the replacement of peripheral monocytes (*53*). For microglial depletion, PLX3397 (Macklin, P872507) was dissolved in 5% dimethyl sulfoxide (DMSO), 45% polyethylene glycol 300 (PEG300), and 50% double-distilled water. The cKO mice received daily treatment with vehicle or PLX (40 mg/kg) by oral gavage for 10 weeks before behavioral tests (*54*, *55*). To investigate the effect of type I IFN signaling in cKO mice, fludarabine (Macklin, F810231) was dissolved in 5% DMSO, 40% PEG300, 5% Tween 80, and 50% double-distilled water. The cKO mice received daily treatment with vehicle or fludarabine (10 mg/kg) by intraperitoneal injections for 10 weeks before behavioral tests (*24*). Mice were sacrificed at different time points during the diet. Mice were maintained under a standard laboratory condition with unlimited access to standard rodent chow and clean water. All animal procedures were performed in accordance with *Guide for the Care and Use of Laboratory Animals* of the School of Medicine, Jiangnan University and approved by the Jiangnan University Animal Experimentations Ethics Committee (JN no: 20171030c0110506).

MWM test

Spatial learning and memory were assessed using the MWM test as previously described (*56*). Briefly, a circular platform (diameter: 11 cm) was hidden 1.5 cm under the water surface in the center of one quadrant of a 120-cm circular pool. Milk powder was added to the water, and the temperature of the pool was maintained at 22° ± 1°C. Habituation training was on day 0. The learning trials were conducted over five consecutive days, with four trial sessions daily. In each trial, mice were put in the water at one of four positions facing the pool wall and was allowed up to 60 s to find the platform. On day 6, the probe test was performed without the platform. Cross platform number was measured to evaluate the capability of spatial memory.

Open-field test

OFT was performed in a 50 cm × 50 cm × 50 cm white square chamber. Each mouse was placed in the center of the open-field apparatus and allowed to explore the arena for 5 min. The data were automatically recorded with a video camera and analyzed by ToxTrac software. The center distance and entries in center area were measured to evaluate anxiety. The chamber was wiped with 70% ethanol before use and before subsequent tests to remove odor cues.

EPM test

The mice were placed at a randomly chosen boundary in the central area of the maze facing one of the open arms and were allowed to explore the arena for 5 min. The data were automatically recorded with a video camera and analyzed by ToxTrac software. The time spent in the open zones of the mazes and entries in open area were measured to evaluate anxiety. The chamber was wiped with 70% ethanol before use and before subsequent tests to remove odor cues.

LDB test

LDB consists of a dark compartment (15 cm × 28 cm × 28 cm) and a bright compartment (30 cm × 28 cm × 28 cm), with a small door between the compartments, which allows one mouse to pass through (*57*, *58*). The animal is placed in the center of the bright box and allowed to explore the arena for 5 min. The number of transitions between compartments and the time spent in the bright box were used to assess anxiety. The chamber was wiped with 70% ethanol before use and before subsequent tests to remove odor cues.

Metabolic phenotype

TC (A111-1-1), TG (A110-1-1), and LDL cholesterol (LDL, A113-1-1) in mice serum were measured using commercial kits (Jiancheng, China). Fasted blood glucose was measured by a glucometer (ACCU-CHEK Performa, Roche) through tail bleeding.

Primary microglia cell

Primary microglia cell was prepared from cerebral cortices of five to eight mice (1 to 2 days old, mixed sex), *Ffar4* KO mice, or controls. As described previously (*51*, *59*, *60*), the cortical tissues were digested with 0.25% trypsin-EDTA for 30 min at 37°C, followed by mechanical triturating in Dulbecco's modified Eagle's medium (DMEM)/F12 with 10% fetal bovine serum (VivaCell, Shanghai, C04001). The mixed cells were passed through a 70-μm cell strainer and plated on poly-D-lysine–coated T25 flasks (NEST Biotechnology, 707003) with DMEM/F12 containing 1% penicillin-streptomycin and 10% fetal bovine serum. After achieving confluency at about 10 days in vitro,

the flasks were shaken (180 rpm) for 1 hour (37°C) to release microglia (microglia are loosely attached to the mixed cell surface layer and can easily be detached from the flask surface by shaking). The supernatant containing the detached microglia was collected and reseeded for 1 to 2 hours to allow microglial attachment. When the cells were attached, they were gently washed with warm 1× phosphate-buffered saline (PBS) twice to remove cell aggregates and cell debris; then, the cells were supplied with fresh culture medium. The microglia were used for experimentation when they reached 60 to 70% confluency.

RNA interference or plasmid transfection

Microglia primary cell or BV2 cells (China Center for Type Culture Collection, Wuhan, China) were grown to 50 to 70% confluence and then transfected with *IFN*-β siRNA (50 pM) or normal control (NC) small interfering RNA (siRNA) (50 pM) using jetPRIME transfection reagent (Polyplus, 114-15) according to the manufacturer's protocol. The siRNA sequences were as follows: mouse *IFN*-β, CAGAATAAACACCTCTGCCAT; mouse *Ffar4*, ACCGCATAGGAGAAATCTCAT; and mouse β-*arrestin-2*, GCCAAGAAGTGTGATAAAGAA. Universal negative control siRNA (GenePharma, A06001) was used as a control. Microglia were stimulated with palmitate (200 μM) for 24 hours, and then type I IFN signaling activation was analyzed. *pcDNA3.1-Ffar4-myc* was used for *Ffar4* overexpression in BV2 cells, and the *pcDNA3.1* empty vector was used as a control.

Microglia isolation

Microglia were isolated by the method described (*61*, *62*). Briefly, mice were anesthetized by isoflurane and perfused with ice-cold saline. Brain tissues were freshly harvested in Hanks' balanced salt solution (HBSS) buffer and then digested in HBSS containing collagenase type 2 (37.5 U/ml) and deoxyribonuclease I (45 U/ml) for 30 min at 37°C. Brain tissue homogenates were filtered with a 70-mm cell strainer and then centrifuged at 600*g* for 5 min (4°C) to collect the cell pellets. Microglia were isolated by density gradient centrifugation. Collected cell pellets were then suspended in 37% Percoll solution. Density gradient was added into 15-ml centrifuge tubes: 70% Percoll, 37% Percoll, and PBS. The density gradient was centrifuged at 800*g* for 30 min (4°C). Microglia were collected at the interface of the bottom two layers (70%/37%). Microglia were further purified by incubating with CD11b MicroBeads (Precision Biomedicals, 721105) according to the manufacturer's protocol.

RNA extraction and RT-qPCR assay

Total RNA was extracted from purified microglia using the FastPure Cell/Tissue Total RNA Isolation Kit V2 (Vazyme, RC112-01). Then, RNA was reverse-transcribed to complementary DNA (cDNA) using the HiScript III 1st Strand cDNA Synthesis Kit (Vazyme, R323-01). RT-qPCR was performed using the Roche LightCycler 480 PCR System and Hieff UNICON qPCR SYBR Green Mastermix (Shanghai YEASEN Biotech, 11198ES). Gene expression of the target genes was evaluated using the $2^{-\Delta\Delta Ct}$ method and normalized to β-*actin*. The RT-qPCR primers are shown in table S1.

Coimmunoprecipitation

BV2 cells were transfected with *myc-Ffar4* plasmid and collected 48 hours after transfection. Cells were lysed with 500 μl of ice-cold IP buffer containing protease inhibitor. The cell lysates were incubated with immunoglobulin G (IgG) and Protein A/G Magnetic Beads (MedChemExpress, HY-K0202) to remove nonspecific reaction. Then, the supernatant after centrifugation was incubated with myc-Tag or β-arrestin-2 antibody and Protein A/G Magnetic Beads overnight at 4°C. The beads were washed three times with lysis buffer and resuspended and boiled in SDS loading buffer. The samples were separated by 10% SDS–polyacrylamide gel electrophoresis (SDS-PAGE) and probed with immunoblotting.

Cleavage under targets and release using nuclease assay

CUT&RUN assay was performed using the Hyperactive pG-MNase CUT&RUN Assay Kit for PCR/qPCR kit (Vazyme, HD101) according to the manufacturer's instructions. Approximately 5×10^5 cells were used for subsequent reactions. The cell samples were incubated with antibodies IgG control and NF-κB (Proteintech, 14220-1-AP) at 4°C overnight and subsequent cleavage and release steps. DNA of CUT&RUN fragments was purified using DNA purification buffers and spin columns. Last, the DNA products were quantified by qPCR, and the primers used are shown in table S1.

RNA sequencing

RNA sequencing (RNA-seq) was performed according to our previous study (*63*). Purified microglia were isolated from five mice in each group. Briefly, total RNA was extracted from purified microglia using FastPure Cell/Tissue Total RNA Isolation Kit V2 (Vazyme, RC112-01). Then, RNA was reverse-transcribed to cDNA using the HiScript III 1st Strand cDNA Synthesis Kit (Vazyme, R312-01/02). The second-strand DNA was performed using the Second Strand cDNA Synthesis Kit (Beyotime Biotechnology, D7172). The second-strand DNA samples were digested and labeled by using Tn5 transposase. Enrichment PCR was performed using HiFi PCR Mix for normal goat serum (CWBIO, CW2648). An Agilent 2100 Bioanalyzer was used to quantify the libraries. Illumina NovaSeq instrument was used to paired-end sequencing of the library (sequencing was performed by GENEWIZ Biotech). Reads were mapped to the mouse genome using STAR (http://code.google.com/p/rna-star/). Differentially expressed genes were defined as a fold change of ≥1.5 with a P value of <0.05. GO enrichment analysis was performed using Metascape (http://metascape.org).

Immunohistochemistry and morphology analysis

Mice were deeply anaesthetized with isoflurane and transcranially perfused with saline, followed by ice-cold 4% paraformaldehyde. Brain tissues were fixed with 4% paraformaldehyde for 24 hours and cryoprotected in 30% sucrose at 4°C for 1 week. The coronal brain sections were cut into 25-μm sections by using cryosection (Leica CM1950, Germany). Sections were blocked with 5% bovine serum albumin in PBS for 2 hours, followed by incubation with anti–Iba-1 (Wako, 019-19741) or CD68 (Bio-Road, MCA1957) for 16 hours (at 4°C). After washing three times in PBS, sections were incubated with Goat Anti-Rabbit IgG H&L (Alexa Fluor 488, Abcam, ab150077) or Goat Anti-Rat IgG H&L (Cy3, Beyotime, A0507) for 1 hour at room temperature. For microglial morphology analysis, images of the dentate gyrus (DG) area were acquired using a confocal laser scanning microscope (Zeiss, LSM 880). Z-stack images containing 8 to 15 steps were taken on a confocal microscope using a 20× objective, and all confocal stacks were acquired at a resolution of 1024 × 1024 pixels with a z-step of 1 μm. Microglial morphology analysis was measured by IMARIS software and ImageJ software.

Enzyme-linked immunosorbent assay

The level of IFN-β in mouse brain hippocampal tissue was measured using the mouse IFN-β ELISA kit (Shanghai Enzyme-linked Biotechnology, ml063095) according to the manufacturer's instructions.

Western blot

Radioimmunoprecipitation assay buffer was used to lyse the total protein from hippocampus or microglia primary cell cultures, and Western blotting was performed as previously described (*64*). Briefly, the protein samples were separated by 10 to 12% SDS-PAGE and transferred to 0.45-mm polyvinylidene difluoride (PVDF) membranes. The membranes were blocked with 5% defatted milk for 60 min and then washed three times with Tris Buffered Saline with Tween 20 (TBST). The PVDF membranes were immunoblotted with primary antibodies: JAK1 (Cell Signaling Technology, 2926), p-JAK1 (Cell Signaling Technology, 3331), Stat1 (Cell Signaling Technology, 9191), p-Stat1 (Cell Signaling Technology, 9172), NF-κB (Cell Signaling Technology, 8242), p–NF-κB (Cell Signaling Technology, 3033), PSD95 (Proteintech, 206651-AP), synaptophysin (Proteintech, 17785-1-AP), cleaved caspase-3 (Cell Signaling Technology, 9661), Bcl-2 (Abcam, 32124), β-arrestin-2 (Proteintech, 10171-1-AP), Myc-Tag (ABclonal, AE010), and β-actin (ABclonal, AC026) at 4°C overnight. Last, the membranes were washed with TBST and incubated with secondary antibodies: anti-rabbit IgG conjugated to horseradish peroxidase (HRP) and anti-mouse IgG conjugated to HRP, at room temperature for 2 hours. The membranes were visualized using an enhanced chemiluminescent reagent (Millipore, WBKLS0500). Quantification of band intensity was performed using ImageJ software.

Statistical analysis

GraphPad Prism 8.0, SPSS 19.0, and R 3.6.0 were used for data analyses. Data are presented as means ± SEM. Statistical significance was determined using two-tailed, unpaired Student's *t* tests for two-group comparisons or one-way analysis of variance (ANOVA) followed by Tukey's post hoc tests for multiple comparisons. Line regression was used to assess the correlation of *Ffar4* expression with inflammatory cytokine expression. MWMs were analyzed by two-way repeated-measures ANOVA, followed by Tukey's post hoc tests. *P* values of <0.05 were considered significant.

Supplementary Materials

This PDF file includes:

Figs. S1 to S8

Table S1

REFERENCES AND NOTES

1. A. J. Lusis, A. D. Attie, K. Reue, Metabolic syndrome: From epidemiology to systems biology. *Nat. Rev. Genet.* **9**, 819–830 (2008).
2. J. J. Noubiap, J. R. Nansseu, E. Lontchi-Yimagou, J. R. Nkeck, U. F. Nyaga, A. T. Ngouo, D. N. Tounouga, F. L. Tianyi, A. J. Foka, A. L. Ndoadoumgue, J. J. Bigna, Global, regional, and country estimates of metabolic syndrome burden in children and adolescents in 2020: A systematic review and modelling analysis. *Lancet Child Adolesc. Health* **6**, 158–170 (2022).
3. G. F. Lewis, R. A. Hegele, Effective, disease-modifying, clinical approaches to patients with mild-to-moderate hypertriglyceridaemia. *Lancet Diabetes Endocrinol.* **10**, 142–148 (2022).
4. T. Scherer, K. Sakamoto, C. Buettner, Brain insulin signalling in metabolic homeostasis and disease. *Nat. Rev. Endocrinol.* **17**, 468–483 (2021).
5. T. V. Rohm, D. T. Meier, J. M. Olefsky, M. Y. Donath, Inflammation in obesity, diabetes, and related disorders. *Immunity* **55**, 31–55 (2022).
6. K. Yaffe, A. Kanaya, K. Lindquist, E. M. Simonsick, T. Harris, R. I. Shorr, F. A. Tylavsky, A. B. Newman, The metabolic syndrome, inflammation, and risk of cognitive decline. *JAMA* **292**, 2237–2242 (2004).
7. T. P. Ng, L. Feng, M. S. Nyunt, L. Feng, Q. Gao, M. L. Lim, S. L. Collinson, M. S. Chong, W. S. Lim, T. S. Lee, P. Yap, K. B. Yap, Metabolic syndrome and the risk of mild cognitive impairment and progression to dementia. *JAMA Neurol.* **73**, 456–463 (2016).
8. M. Kivimaki, A. Singh-Manoux, J. Pentti, S. Sabia, S. T. Nyberg, L. Alfredsson, M. Goldberg, A. Knutsson, M. Koskenvuo, A. Koskinen, A. Kouvonen, M. Nordin, T. Oksanen, T. Strandberg, S. B. Suominen, T. Theorell, J. Vahtera, A. Vaananen, M. Virtanen, P. Westerholm, H. Westerlund, M. Zins, S. Seshadri, G. D. Batty, P. N. Sipila, M. J. Shipley, J. V. Lindbohm, J. E. Ferrie, M. Jokela, IPD-Work consortium, Physical inactivity, cardiometabolic disease, and risk of dementia: An individual-participant meta-analysis. *BMJ* **365**, l1495 (2019).
9. A. Wieckowska-Gacek, A. Mietelska-Porowska, M. Wydrych, U. Wojda, Western diet as a trigger of Alzheimer's disease: From metabolic syndrome and systemic inflammation to neuroinflammation and neurodegeneration. *Ageing Res. Rev.* **70**, 101397 (2021).
10. N. Gomes Goncalves, N. Vidal Ferreira, N. Khandpur, E. Martinez Steele, R. Bertazzi Levy, P. Andrade Lotufo, I. M. Bensenor, P. Caramelli, S. M. Alvim de Matos, D. M. Marchioni, C. K. Suemoto, Association between consumption of ultraprocessed foods and cognitive decline. *JAMA Neurol.* **80**, 142–150 (2023).
11. J. S. Smith, T. F. Pack, A. Inoue, C. Lee, K. Zheng, I. Choi, D. S. Eiger, A. Warman, X. Xiong, Z. Ma, G. Viswanathan, I. M. Levitan, L. K. Rochelle, D. P. Staus, J. C. Snyder, A. W. Kahsai, M. G. Caron, S. Rajagopal, Noncanonical scaffolding of Gαi and β-arrestin by G protein-coupled receptors. *Science* **371**, eaay1833 (2021).
12. A. P. Campbell, A. V. Smrcka, Targeting G protein-coupled receptor signalling by blocking G proteins. *Nat. Rev. Drug Discov.* **17**, 789–803 (2018).
13. T. Ikeda, A. Nishida, M. Yamano, I. Kimura, Short-chain fatty acid receptors and gut microbiota as therapeutic targets in metabolic, immune, and neurological diseases. *Pharmacol. Ther.* **239**, 108273 (2022).
14. G. Milligan, B. Shimpukade, T. Ulven, B. D. Hudson, Complex pharmacology of free fatty acid receptors. *Chem. Rev.* **117**, 67–110 (2017).
15. I. Kimura, A. Ichimura, R. Ohue-Kitano, M. Igarashi, Free fatty acid receptors in health and disease. *Physiol. Rev.* **100**, 171–210 (2020).
16. S. Zhu, J. Zhang, X. Jiang, W. Wang, Y. Q. Chen, Free fatty acid receptor 4 deletion attenuates colitis by modulating T_{reg} cells via ZBED6-IL33 pathway. *EBioMedicine* **80**, 104060 (2022).
17. W. Yang, H. Liu, L. Xu, T. Yu, X. Zhao, S. Yao, Q. Zhao, S. Barnes, S. M. Cohn, S. M. Dann, H. Zhang, X. Zuo, Y. Li, Y. Cong, GPR120 inhibits colitis through regulation of $CD4^+$ T cell interleukin 10 production. *Gastroenterology* **162**, 150–165 (2022).
18. T. Quesada-Lopez, R. Cereijo, J. V. Turatsinze, A. Planavila, M. Cairo, A. Gavalda-Navarro, M. Peyrou, R. Moure, R. Iglesias, M. Giralt, D. L. Eizirik, F. Villarroya, The lipid sensor GPR120 promotes brown fat activation and FGF21 release from adipocytes. *Nat. Commun.* **7**, 13479 (2016).
19. P. T. Tseng, B. S. Zeng, M. W. Suen, Y. C. Wu, C. U. Correll, B. Y. Zeng, J. S. Kuo, Y. W. Chen, T. Y. Chen, Y. K. Tu, P. Y. Lin, A. F. Carvalho, B. Stubbs, D. J. Li, C. S. Liang, C. W. Hsu, C. K. Sun, Y. S. Cheng, P. Y. Yeh, M. K. Wu, Y. L. Shiue, K. P. Su, Efficacy and acceptability of anti-inflammatory eicosapentaenoic acid for cognitive function in Alzheimer's dementia: A network meta-analysis of randomized, placebo-controlled trials with omega-3 fatty acids and FDA-approved pharmacotherapy. *Brain Behav. Immun.* **111**, 352–364 (2023).
20. R. P. Bazinet, S. Laye, Polyunsaturated fatty acids and their metabolites in brain function and disease. *Nat. Rev. Neurosci.* **15**, 771–785 (2014).
21. G. Boden, C. Homko, C. A. Barrero, T. P. Stein, X. Chen, P. Cheung, C. Fecchio, S. Koller, S. Merali, Excessive caloric intake acutely causes oxidative stress, GLUT4 carbonylation, and insulin resistance in healthy men. *Sci. Transl. Med.* **7**, 304re307 (2015).
22. N. R. V. Dragano, C. Solon, A. F. Ramalho, R. F. de Moura, D. S. Razolli, E. Christiansen, C. Azevedo, T. Ulven, L. A. Velloso, Polyunsaturated fatty acid receptors, GPR40 and GPR120, are expressed in the hypothalamus and control energy homeostasis and inflammation. *J. Neuroinflammation* **14**, 91 (2017).
23. Z. Ren, L. Chen, Y. Wang, X. Wei, S. Zeng, Y. Zheng, C. Gao, H. Liu, Activation of the omega-3 fatty acid receptor GPR120 protects against focal cerebral ischemic injury by preventing inflammation and apoptosis in mice. *J. Immunol.* **202**, 747–759 (2019).
24. Y. Zhao, C. Ma, C. Chen, S. Li, Y. Wang, T. Yang, R. A. Stetler, M. V. L. Bennett, C. E. Dixon, J. Chen, Y. Shi, STAT1 contributes to microglial/macrophage inflammation and neurological dysfunction in a mouse model of traumatic brain injury. *J. Neurosci.* **42**, 7466–7481 (2022).
25. H. Xiu, J. Gong, T. Huang, Y. Peng, S. Bai, G. Xiong, S. Zhang, H. Huang, Z. Cai, G. Zhang, Fludarabine inhibits type I interferon-induced expression of the SARS-CoV-2 receptor angiotensin-converting enzyme 2. *Cell. Mol. Immunol.* **18**, 1829–1831 (2021).
26. Y. Yu, S. Dou, P. Peng, L. Ma, X. Qi, T. Liu, Y. Yu, C. Wei, W. Shi, Targeting type I IFN/STAT1 signaling inhibited and reversed corneal squamous metaplasia in Aire-deficient mouse. *Pharmacol. Res.* **187**, 106615 (2023).
27. K. J. Spiller, C. R. Restrepo, T. Khan, M. A. Dominique, T. C. Fang, R. G. Canter, C. J. Roberts, K. R. Miller, R. M. Ransohoff, J. Q. Trojanowski, V. M. Lee, Microglia-mediated recovery from ALS-relevant motor neuron degeneration in a mouse model of TDP-43 proteinopathy. *Nat. Neurosci.* **21**, 329–340 (2018).

28. S. Qiu, J. P. Palavicini, J. Wang, N. S. Gonzalez, S. He, E. Dustin, C. Zou, L. Ding, A. Bhattacharjee, C. E. Van Skike, V. Galvan, J. L. Dupree, X. Han, Adult-onset CNS myelin sulfatide deficiency is sufficient to cause Alzheimer's disease-like neuroinflammation and cognitive impairment. *Mol. Neurodegener.* **16**, 64 (2021).
29. J. P. Chadarevian, S. I. Lombroso, G. C. Peet, J. Hasselmann, C. Tu, D. E. Marzan, J. Capocchi, F. S. Purnell, K. M. Nemec, A. Lahian, A. Escobar, W. England, S. Chaluvadi, C. A. O'Brien, F. Yaqoob, W. H. Aisenberg, M. Porras-Paniagua, M. L. Bennett, H. Davtyan, R. C. Spitale, M. Blurton-Jones, F. C. Bennett, Engineering an inhibitor-resistant human CSF1R variant for microglia replacement. *J. Exp. Med.* **220**, e20220857 (2023).
30. A. Tripathi, C. Whitehead, K. Surrao, A. Pillai, A. Madeshiya, Y. Li, H. Khodadadi, A. O. Ahmed, G. Turecki, B. Baban, A. Pillai, Type 1 interferon mediates chronic stress-induced neuroinflammation and behavioral deficits via complement component 3-dependent pathway. *Mol. Psychiatry* **26**, 3043–3059 (2021).
31. Y. Q. Du, X. Y. Sha, J. Cheng, J. Wang, J. Y. Lin, W. T. An, W. Pan, L. J. Zhang, X. N. Tao, Y. F. Xu, Y. L. Jia, Z. Yang, P. Xiao, M. Liu, J. P. Sun, X. Yu, Endogenous lipid-GPR120 signaling modulates pancreatic islet homeostasis to different extents. *Diabetes* **71**, 1454–1471 (2022).
32. Y. Yan, W. Jiang, T. Spinetti, A. Tardivel, R. Castillo, C. Bourquin, G. Guarda, Z. Tian, J. Tschopp, R. Zhou, Omega-3 fatty acids prevent inflammation and metabolic disorder through inhibition of NLRP3 inflammasome activation. *Immunity* **38**, 1154–1163 (2013).
33. D. Y. Oh, S. Talukdar, E. J. Bae, T. Imamura, H. Morinaga, W. Fan, P. Li, W. J. Lu, S. M. Watkins, J. M. Olefsky, GPR120 is an omega-3 fatty acid receptor mediating potent anti-inflammatory and insulin-sensitizing effects. *Cell* **142**, 687–698 (2010).
34. S. Kullmann, M. Heni, M. Hallschmid, A. Fritsche, H. Preissl, H. U. Haring, Brain insulin resistance at the crossroads of metabolic and cognitive disorders in humans. *Physiol. Rev.* **96**, 1169–1209 (2016).
35. V. Frisardi, V. Solfrizzi, D. Seripa, C. Capurso, A. Santamato, D. Sancarlo, G. Vendemiale, A. Pilotto, F. Panza, Metabolic-cognitive syndrome: A cross-talk between metabolic syndrome and Alzheimer's disease. *Ageing Res. Rev.* **9**, 399–417 (2010).
36. H. A. Bischoff-Ferrari, B. Vellas, R. Rizzoli, R. W. Kressig, J. A. P. da Silva, M. Blauth, D. T. Felson, E. V. M. Closkey, B. Watzl, L. C. Hofbauer, D. Felsenberg, W. C. Willett, B. Dawson-Hughes, J. E. Manson, U. Siebert, R. Theiler, H. B. Staehelin, C. de Godoi Rezende Costa Molino, P. O. Chocano-Bedoya, L. A. Abderhalden, A. Egli, J. A. Kanis, E. J. Orav, DO-HEALTH Research Group, Effect of vitamin d supplementation, omega-3 fatty acid supplementation, or a strength-training exercise program on clinical outcomes in older adults: The do-health randomized clinical trial. *JAMA* **324**, 1855–1868 (2020).
37. E. Y. Chew, T. E. Clemons, E. Agron, L. J. Launer, F. Grodstein, P. S. Bernstein, Age-Related Eye Disease Study 2 (AREDS2) Research Group, Effect of omega-3 fatty acids, lutein/zeaxanthin, or other nutrient supplementation on cognitive function. *JAMA* **314**, 791–801 (2015).
38. H. T. Lai, M. C. de Oliveira Otto, R. N. Lemaitre, B. McKnight, X. Song, I. B. King, P. H. Chaves, M. C. Odden, A. B. Newman, D. S. Siscovick, D. Mozaffarian, Serial circulating omega 3 polyunsaturated fatty acids and healthy ageing among older adults in the Cardiovascular Health Study: Prospective cohort study. *BMJ* **363**, k4067 (2018).
39. M. Burckhardt, M. Herke, T. Wustmann, S. Watzke, G. Langer, A. Fink, Omega-3 fatty acids for the treatment of dementia. *Cochrane Database Syst. Rev.* **4**, CD009002 (2016).
40. J. F. Quinn, R. Raman, R. G. Thomas, K. Yurko-Mauro, E. B. Nelson, C. Van Dyck, J. E. Galvin, J. Emond, C. R. Jack Jr., M. Weiner, L. Shinto, P. S. Aisen, Docosahexaenoic acid supplementation and cognitive decline in Alzheimer disease: A randomized trial. *JAMA* **304**, 1903–1911 (2010).
41. A. Ichimura, A. Hirasawa, O. Poulain-Godefroy, A. Bonnefond, T. Hara, L. Yengo, I. Kimura, A. Leloire, N. Liu, K. Iida, H. Choquet, P. Besnard, C. Lecoeur, S. Vivequin, K. Ayukawa, M. Takeuchi, K. Ozawa, M. Tauber, C. Maffeis, A. Morandi, R. Buzzetti, P. Elliott, A. Pouta, M. R. Jarvelin, A. Korner, W. Kiess, M. Pigeyre, R. Caiazzo, W. Van Hul, L. Van Gaal, F. Horber, B. Balkau, C. Levy-Marchal, K. Rouskas, A. Kouvatsi, J. Hebebrand, A. Hinney, A. Scherag, F. Pattou, D. Meyre, T. A. Koshimizu, I. Wolowczuk, G. Tsujimoto, P. Froguel, Dysfunction of lipid sensor GPR120 leads to obesity in both mouse and human. *Nature* **483**, 350–354 (2012).
42. A. Bonnefond, A. Lamri, A. Leloire, E. Vaillant, R. Roussel, C. Levy-Marchal, J. Weill, P. Galan, S. Hercberg, S. Ragot, S. Hadjadj, G. Charpentier, B. Balkau, M. Marre, F. Fumeron, P. Froguel, Contribution of the low-frequency, loss-of-function p.R270H mutation in FFAR4 (GPR120) to increased fasting plasma glucose levels. *J. Med. Genet.* **52**, 595–598 (2015).
43. C. Mao, P. Xiao, X. N. Tao, J. Qin, Q. T. He, C. Zhang, S. C. Guo, Y. Q. Du, L. N. Chen, D. D. Shen, Z. S. Yang, H. Q. Zhang, S. M. Huang, Y. H. He, J. Cheng, Y. N. Zhong, P. Shang, J. Chen, D. L. Zhang, Q. L. Wang, M. X. Liu, G. Y. Li, Y. Guo, H. E. Xu, C. Wang, C. Zhang, S. Feng, X. Yu, Y. Zhang, J. P. Sun, Unsaturated bond recognition leads to biased signal in a fatty acid receptor. *Science* **380**, eadd6220 (2023).
44. A. Hirasawa, K. Tsumaya, T. Awaji, S. Katsuma, T. Adachi, M. Yamada, Y. Sugimoto, S. Miyazaki, G. Tsujimoto, Free fatty acids regulate gut incretin glucagon-like peptide-1 secretion through GPR120. *Nat. Med.* **11**, 90–94 (2005).
45. K. Timper, A. Del Rio-Martin, A. L. Cremer, S. Bremser, J. Alber, P. Giavalisco, L. Varela, C. Heilinger, H. Nolte, A. Trifunovic, T. L. Horvath, P. Kloppenburg, H. Backes, J. C. Bruning, GLP-1 receptor signaling in astrocytes regulates fatty acid oxidation, mitochondrial integrity, and function. *Cell Metab.* **31**, 1189–1205.e13 (2020).
46. G. Muscogiuri, R. A. DeFronzo, A. Gastaldelli, J. J. Holst, Glucagon-like peptide-1 and the central/peripheral nervous system: Crosstalk in diabetes. *Trends Endocrinol. Metab.* **28**, 88–103 (2017).
47. C. H. Norgaard, S. Friedrich, C. T. Hansen, T. Gerds, C. Ballard, D. V. Moller, L. B. Knudsen, K. Kvist, B. Zinman, E. Holm, C. Torp-Pedersen, L. S. Morch, Treatment with glucagon-like peptide-1 receptor agonists and incidence of dementia: Data from pooled double-blind randomized controlled trials and nationwide disease and prescription registers. *Alzheimers Dement.* **8**, e12268 (2022).
48. K. Iwasa, S. Yamamoto, K. Yamashina, N. Yagishita-Kyo, K. Maruyama, T. Awaji, Y. Takei, A. Hirasawa, K. Yoshikawa, A peripheral lipid sensor GPR120 remotely contributes to suppression of PGD(2)-microglia-provoked neuroinflammation and neurodegeneration in the mouse hippocampus. *J. Neuroinflammation* **18**, 304 (2021).
49. L. Catrysse, G. van Loo, Inflammation and the metabolic syndrome: The tissue-specific functions of NF-κB. *Trends Cell Biol.* **27**, 417–429 (2017).
50. R. Freitas, C. A. M. Fraga, NF-κB-IKKβ pathway as a target for drug development: Realities, challenges and perspectives. *Curr. Drug Targets* **19**, 1933–1942 (2018).
51. J. D. Kim, N. A. Yoon, S. Jin, S. Diano, Microglial UCP2 mediates inflammation and obesity induced by high-fat feeding. *Cell Metab.* **30**, 952–962.e5 (2019).
52. X. L. Wang, S. Kooijman, Y. Gao, L. Tzeplaeff, B. Cosquer, I. Milanova, S. E. C. Wolff, N. Korpel, M. F. Champy, B. Petit-Demouliere, I. Goncalves Da Cruz, T. Sorg-Guss, P. C. N. Rensen, J. C. Cassel, A. Kalsbeek, A. L. Boutillier, C. X. Yi, Microglia-specific knock-down of Bmal1 improves memory and protects mice from high fat diet-induced obesity. *Mol. Psychiatry* **26**, 6336–6349 (2021).
53. M. Valdearcos, J. D. Douglass, M. M. Robblee, M. D. Dorfman, D. R. Stifler, M. L. Bennett, I. Gerritse, R. Fasnacht, B. A. Barres, J. P. Thaler, S. K. Koliwad, Microglial inflammatory signaling orchestrates the hypothalamic immune response to dietary excess and mediates obesity susceptibility. *Cell Metab.* **27**, 1356 (2018).
54. D. Zhang, S. Li, L. Hou, L. Jing, Z. Ruan, B. Peng, X. Zhang, J. S. Hong, J. Zhao, Q. Wang, Microglial activation contributes to cognitive impairments in rotenone-induced mouse Parkinson's disease model. *J. Neuroinflammation* **18**, 4 (2021).
55. Y. J. Liang, S. Y. Feng, Y. P. Qi, K. Li, Z. R. Jin, H. B. Jing, L. Y. Liu, J. Cai, G. G. Xing, K. Y. Fu, Contribution of microglial reaction to increased nociceptive responses in high-fat-diet (HFD)-induced obesity in male mice. *Brain Behav. Immun.* **80**, 777–792 (2019).
56. K. Bromley-Brits, Y. Deng, W. Song, Morris water maze test for learning and memory deficits in Alzheimer's disease model mice. *J. Vis. Exp.*, 2920 (2011).
57. Y. D. Li, Y. J. Luo, W. Xu, J. Ge, Y. Cherasse, Y. Q. Wang, M. Lazarus, W. M. Qu, Z. L. Huang, Ventral pallidal GABAergic neurons control wakefulness associated with motivation through the ventral tegmental pathway. *Mol. Psychiatry* **26**, 2912–2928 (2021).
58. S. Erhardt, A. Pocivavsek, M. Repici, X. C. Liu, S. Imbeault, D. C. Maddison, M. A. R. Thomas, J. L. Smalley, M. K. Larsson, P. J. Muchowski, F. Giorgini, R. Schwarcz, Adaptive and behavioral changes in kynurenine 3-monooxygenase knockout mice: Relevance to psychotic disorders. *Biol. Psychiatry* **82**, 756–765 (2017).
59. L. Lin, R. Desai, X. Wang, E. H. Lo, C. Xing, Characteristics of primary rat microglia isolated from mixed cultures using two different methods. *J. Neuroinflammation* **14**, 101 (2017).
60. S. Du, S. Xiong, X. Du, T. F. Yuan, B. Peng, Y. Rao, Primary microglia isolation from postnatal mouse brains. *J. Vis. Exp.* **168**, e62237 (2021).
61. M. Sato-Hashimoto, T. Nozu, R. Toriba, A. Horikoshi, M. Akaike, K. Kawamoto, A. Hirose, Y. Hayashi, H. Nagai, W. Shimizu, A. Saiki, T. Ishikawa, R. Elhanbly, T. Kotani, Y. Murata, Y. Saito, M. Naruse, K. Shibasaki, P. A. Oldenborg, S. Jung, T. Matozaki, Y. Fukazawa, H. Ohnishi, Microglial SIRPα regulates the emergence of $CD11c^{+}$ microglia and demyelination damage in white matter. *eLife* **8**, e42025 (2019).
62. D. Sommer, I. Corstjens, S. Sanchez, D. Dooley, S. Lemmens, J. Van Broeckhoven, J. Bogie, T. Vanmierlo, P. M. Vidal, S. Rose-John, M. Gou-Fabregas, S. Hendrix, ADAM17-deficiency on microglia but not on macrophages promotes phagocytosis and functional recovery after spinal cord injury. *Brain Behav. Immun.* **80**, 129–145 (2019).
63. S. Zhu, W. Wang, J. Zhang, S. Ji, Z. Jing, Y. Q. Chen, Slc25a5 regulates adipogenesis by modulating ERK signaling in OP9 cells. *Cell. Mol. Biol. Lett.* **27**, 11 (2022).
64. X. Jiang, S. Ji, F. Yuan, T. Li, S. Cui, W. Wang, X. Ye, R. Wang, Y. Chen, S. Zhu, Pyruvate dehydrogenase B regulates myogenic differentiation via the FoxP1-Arih2 axis. *J. Cachexia Sarcopenia Muscle* **14**, 606–621 (2023).

Acknowledgments: We thank C. X. Tang form Xuzhou Medical University for providing the Cx3cr1-CreER mice. We thank members of Y.Q.C. laboratories for helpful discussions. All schematics were generated using BioRender and Figdraw. **Funding:** This work was supported by the National Natural Science Foundation of China (82000808 and 82000685) and the Wuxi Taihu Lake Talent Plan, Supports for Leading Talents in Medical and Health Profession. **Author contributions:** Conceptualization: W.W., Y.Q.C., and S.Z. Data curation: W.W., Jiayu Li, S.C., X.Y., Z.W., T.Z., X.J., Y.K., and X.C. Formal analysis: W.W., Jinyou Li, S.C., X.Y., Z.W., T.Z., X.J., Y.K., and X.C. Funding acquisition: Jinyou Li. and S.Z. Investigation: W.W., Jinyou Li, S.C., X.Y., Z.W., Y.Q.C., and S.Z. Methodology: W.W., Jiayu Li, S.C., X.Y., Z.W., T.Z., X.J., Y.K., and X.C. Project administration: Jinyou Li and S.Z. Supervision: W.W., Jinyou Li, Y.Q.C., and S.Z. Validation: W.W., Jinyou Li, T.Z., X.J., Y.K., Y.Q.C., and S.Z. Visualization: W.W., Jinyou Li, T.Z., X.J., Y.K., Y.Q.C., and S.Z. Writing—original draft: W.W., Jinyou Li, Z.W., T.Z., Y.Q.C., and S.Z. Writing—review and editing: W.W.,

Jinyou Li, Z.W., T.Z., Y.Q.C., and S.Z. All authors read and approved the final manuscript. **Competing interests:** The authors declare that they have no competing interests. **Data and materials availability:** All data needed to evaluate the conclusions in the paper are present in the paper and/or the Supplementary Materials.

Submitted 16 July 2023
Accepted 3 January 2024
Published 2 February 2024
10.1126/sciadv.adj7813